ICARUS 121, 249–274 (1996)
ARTICLE NO. 0084

Cometary Nuclei and Tidal Disruption: The Geologic Record of Crater Chains on Callisto and Ganymede

PAUL M. SCHENK

Lunar and Planetary Institute, 3600 Bay Area Boulevard, Houston, Texas 77058
E-mail: schenk@lpi.jsc.nasa.gov

ERIK ASPHAUG

NASA Ames Research Center, Moffett Field, California 94035

WILLIAM B. MCKINNON

Department of Earth and Planetary Sciences and McDonnell Center for the Space Sciences, Washington University, Saint Louis, Missouri 63130

H. J. MELOSH

Lunar and Planetary Laboratory, University of Arizona, Tucson, Arizona 85721

AND

PAUL R. WEISSMAN

Jet Propulsion Laboratory Pasadena, California 91109

Received August 7, 1995; revised March 5, 1996

Prominent crater chains on Ganymede and Callisto are most likely the impact scars of comets tidally disrupted by Jupiter and are not secondary crater chains. We have examined the morphology of these chains in detail in order to place constraints on the properties of the comets that formed them and the disruption process. In these chains, intercrater spacing varies by no more than a factor of 2 and the craters within a given chain show almost no deviation from linearity (although the chains themselves are on gently curved small circles). All of these crater chains occur on or very near the Jupiter-facing hemisphere. For a given chain, the estimated masses of the fragments that formed each crater vary by no more than an order of magnitude. The mean fragment masses for all the chains vary by over four orders of magnitude (W. B. McKinnon and P. M. Schenk 1995, *Geophys. Res. Lett.* 13, 1829–1832), however. The mass of the parent comet for each crater chain is not correlated with the number of fragments produced during disruption but is correlated with the mean mass of the fragments produced in a given disruption event. Also, the larger fragments are located near the center of each chain. All of these characteristics are consistent with those predicted by disruption simulations based on the rubble pile cometary nucleus model (in which nuclei are composed on numerous small fragments weakly bound by self-gravity), and with those observed in Comet D/Shoemaker–Levy 9. Similar crater chains have not been found on the other icy satellites, but the impact record of disrupted comets on Callisto and Ganymede indicates that disruption events occur within the Jupiter system roughly once every 200 to 400 years.

INTRODUCTION

Shortly after the discovery of disrupted comet D/Shoemaker–Levy 9 (S–L9) in 1993, Melosh and Schenk (1993) recognized the startling similarity between the S–L9 fragment train and prominent linear crater chains on the Galilean satellites Callisto and Ganymede (Fig. 1). They proposed that these crater chains are impact scars of past tidally disrupted comets. If this hypothesis is correct, the study of these crater chains offers a unique opportunity to investigate the properties of comets and cometary fragments. These chains also provide new constraints on models for how comets are constructed and the process of cometary disruption. Are comets constructed of "rubble piles" (Donn *et al.* 1985, Weissman 1986) or are they homogeneous "solid" snowballs (e.g., Sekanina 1996)? The crater chain record is also important for placing the disruption

0019-1035/96 $18.00

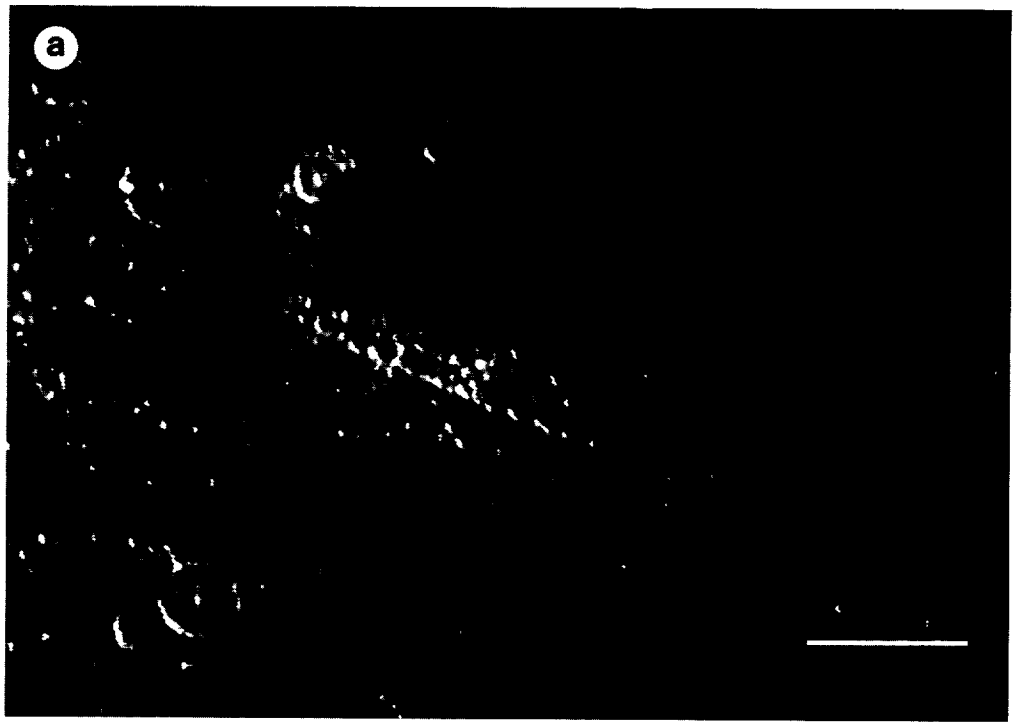

FIG. 1. Crater chains on (a–h) Callisto, and (j–l) Ganymede. Each image is in orthographic projection at 0.9 km/pixel resolution. Figure labels (a–l) correspond sequentially to the labels for crater chains in Table I. Arrow in (b) points to lateral ridge bisecting crater in Gipul Catena. Image frame numbers are listed in Table I. Chain locations are also mapped in Figs. 4, and 7. Image in (f) is smeared due to camera motion; faint streaks in (d) are also due to smear. North is up in all images. Scale bars are 100 km.

of S–L9 and its collision with Jupiter in 1994 in historical context.

Only two tidally disrupted comets have been observed in space. During a very close pass to Jupiter ($\sim$1.3 R_J) in July 1992, S–L9 broke up into a linear "string of pearls" consisting of at least 21 fragments. P/Brooks 2 passed within $\sim$2 R_J of Jupiter in 1886 and apparently broke up (Sekanina and Yeomans 1985). This comet was not discovered as a multiple comet until 1889, and unlike S–L9, was not subject to intense scrutiny by modern instrumentation and little can be said about its properties. At least 11 prominent crater chains have been identified on Ganymede and Callisto (see below), potentially increasing by an order of magnitude the sample of historical tidally disrupted comets for which we have useful observational constraints.

Previous work by some of us (Melosh and Schenk 1993) showed that disrupted comets can account for crater chains of the lengths observed and their occurrence on the Jupiter-facing hemispheres of Ganymede and Callisto. McKinnon and Schenk (1995) estimated the masses and diameters of the projectiles responsible for forming these craters. In this report, we describe in detail the morphology of these crater chains and of the craters that compose them. These include measurements of crater size and intercrater spacing, crater chain location and curvature, and the number of craters in each chain, and a search for correlations between these and other properties. These data confirm that impact of tidally disrupted comets is the most likely explanation for most of these chains. From the crater chain record, we estimate the frequency of cometary disruption events in the jovian system. We compare the morphology of these crater chains (and the comets that produced them) with the observed properties of the S–L9 fragment train (e.g., Weaver *et al.* 1994, 1995), and with the properties of disrupted comets predicted from models of cometary nuclei, especially the rubble pile model (e.g., Asphaug and Benz 1994, 1996, Solem 1994, Olson and Mumma 1994; Rettig *et al.* 1994, Richardson *et al.* 1995). The detailed morphology of crater chains should also provide useful constraints for future models of cometary disruption.

MORPHOLOGY OF CRATER CHAINS

Passey and Shoemaker (1982) identified 5 prominent crater chains (or catenae) on Callisto, consisting of strings of closely spaced roughly similar-sized aligned craters. They concluded that these chains were formed by impact of secondary ejecta from large basins, possibly Valhalla for two chains. Melosh and Schenk (1993) identified a total of 13 crater chains on Callisto and three previously

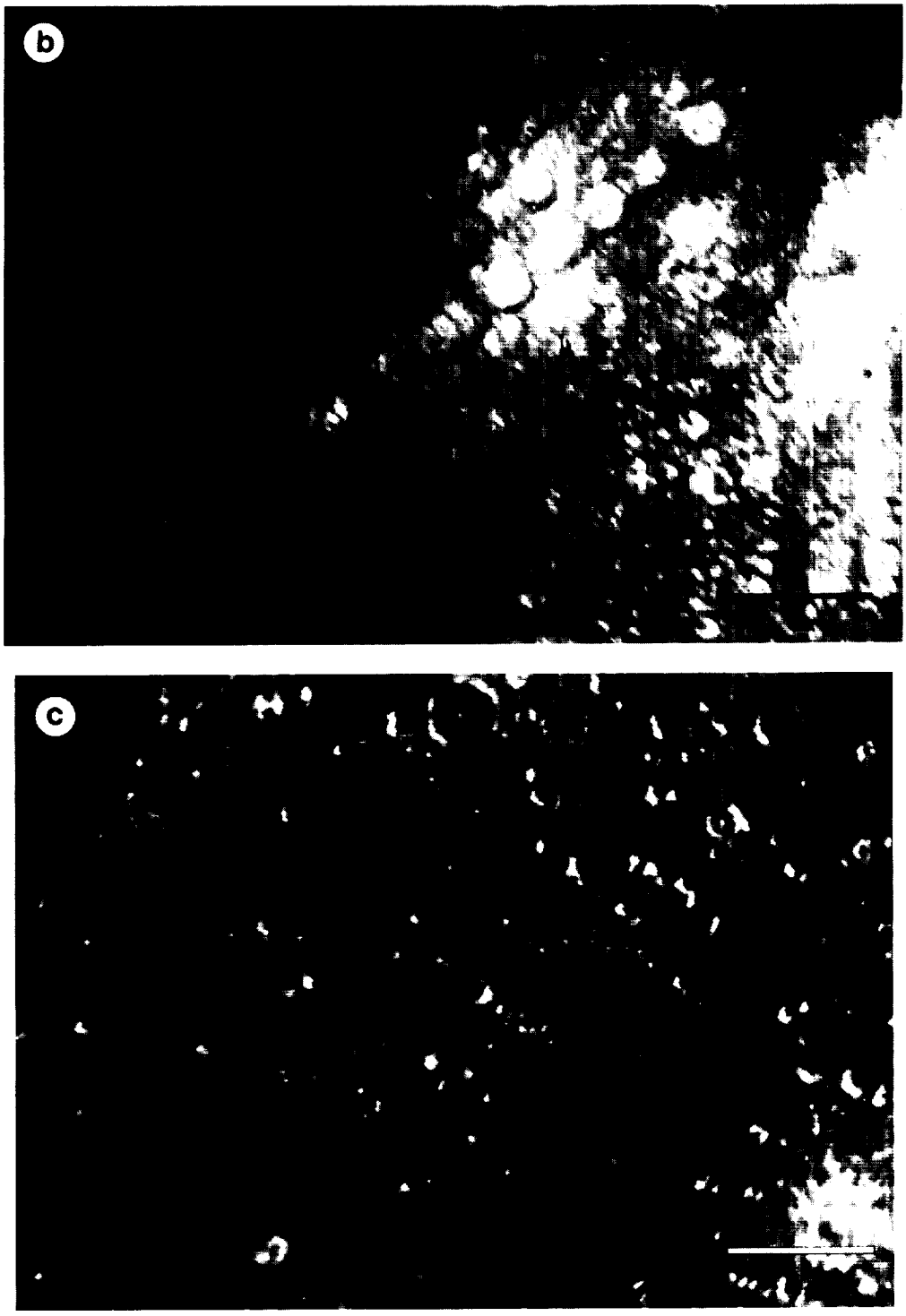

FIG. 1—*Continued*

unrecognized crater chains on Ganymede, but were unable to link any of these directly to any specific basin. We have examined these chains in detail and confirm a total of eight prominent crater chains on Callisto, and 3 on Ganymede (Fig. 1, Table I). Three of the features identified on Callisto by Melosh and Schenk are more accurately described as groove-like structures. These are within the outer ring zone of the Valhalla multiring impact basin and are either radial or concentric to it, and are probably tectonic features associated with the formation of Valhalla. Also, one of their

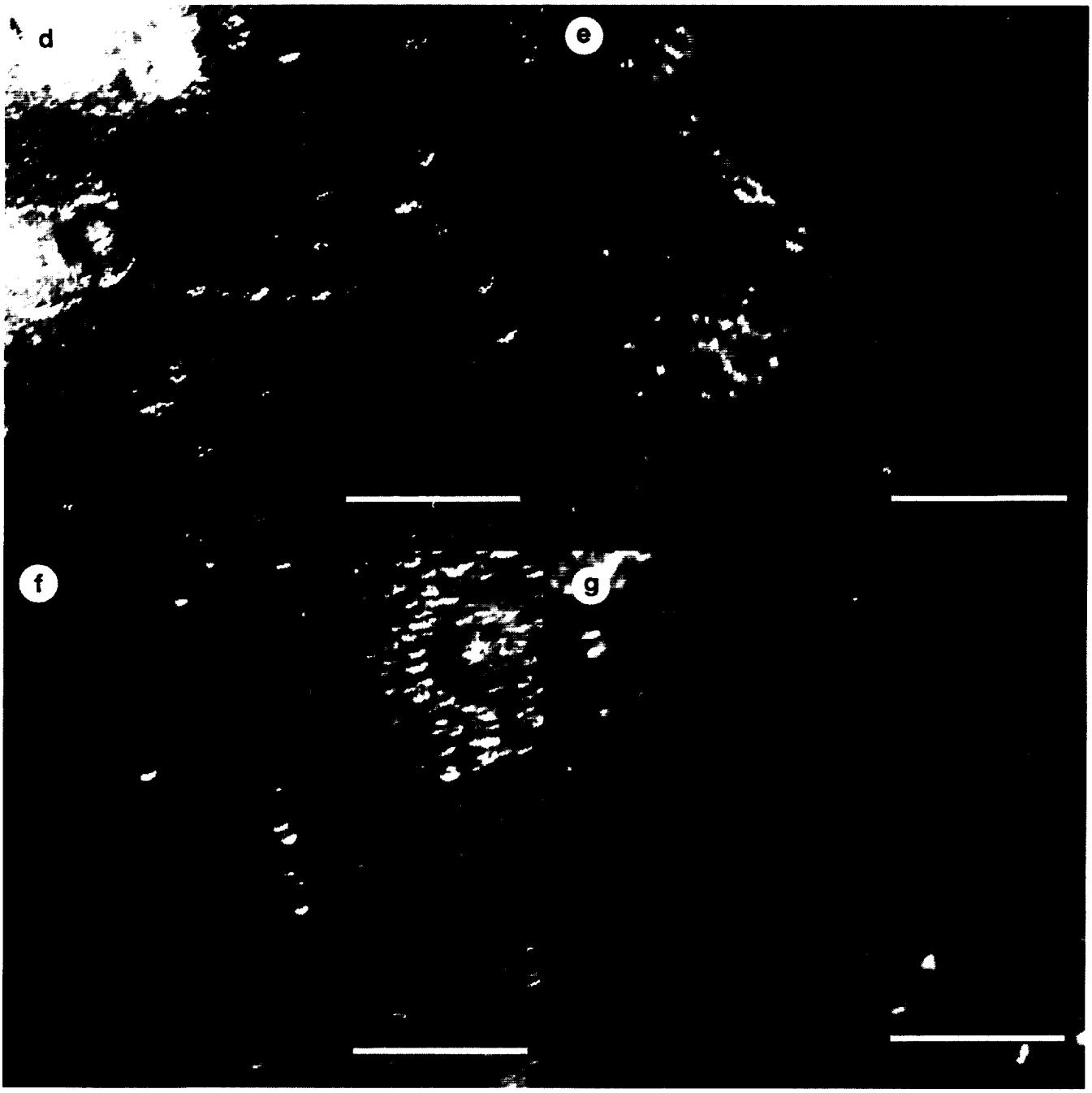

FIG. 1—*Continued*

crater chains is probably a secondary chain associated with the Valhalla basin (see below). We note that variations in viewing geometry and solar illumination, and differences in Voyager image resolution of a factor of two are present in the data set. As a result, some crater chains, notably Enki and Gunntro Catenae, were seen more poorly. Also, all images of Sid Catena on Callisto were smeared by camera motion and data on this chain are of lower quality. The abundance of linear tectonic features makes crater chains more difficult to recognize on Ganymede. Despite these issues, the 11 crater chains on Callisto and Ganymede identified here are composed of distinct crater forms and are prominent features on these satellites (Fig. 1).

Crater Morphology

Catena craters are circular or slightly elliptical and have raised rims and central peaks (Figs. 1, 2), morphologies

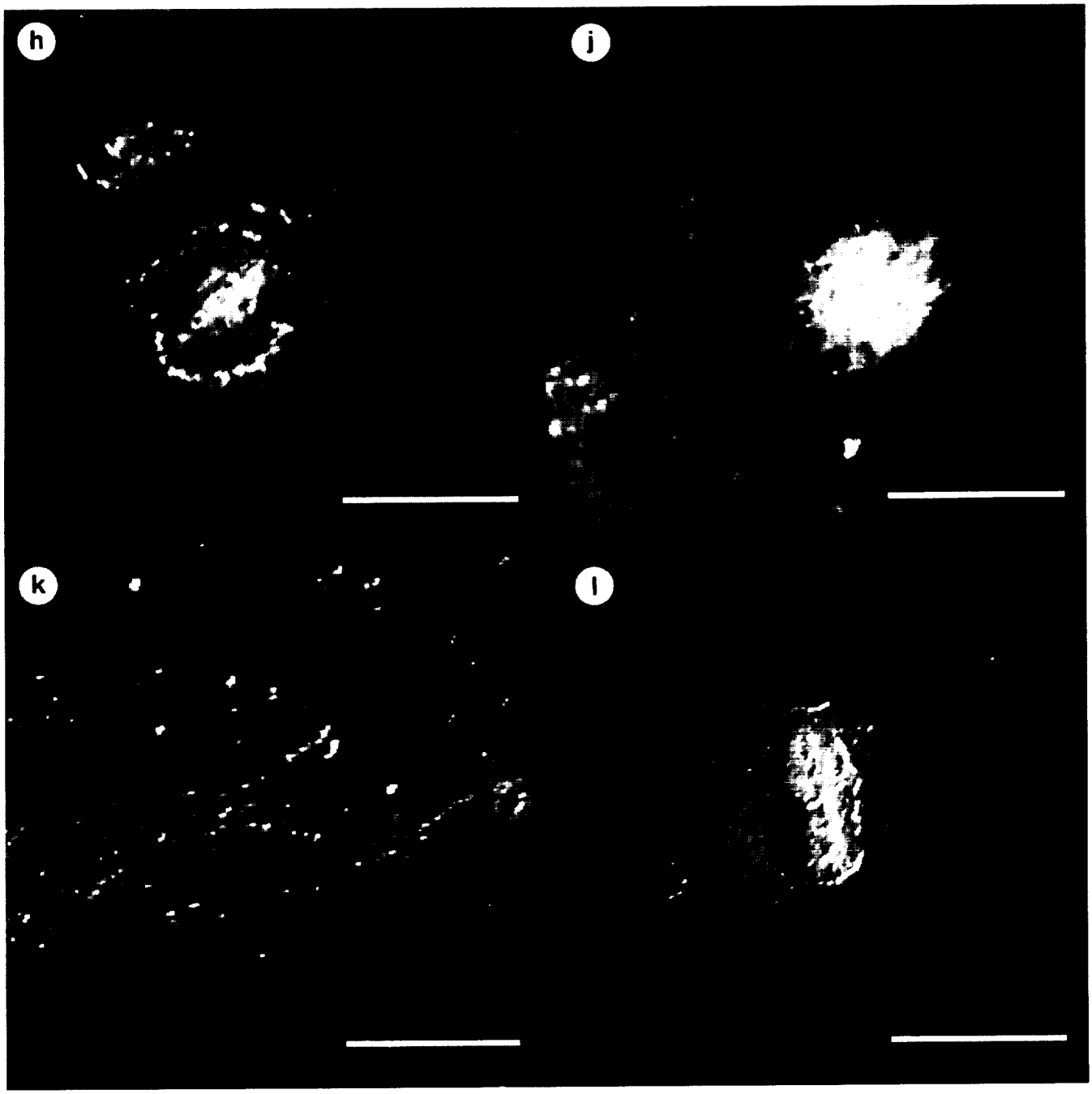

FIG. 1—*Continued*

indicative of impact (Passey and Shoemaker 1982). Catena craters larger than ~30 km usually have flat floors and/or central pits (Fig. 1a), as expected for impact craters of this size (Passey and Shoemaker 1982, Schenk 1993). Enki and Nanshe Catenae on Ganymede (Figs. 1j, 1l) also have distinct bright ejecta deposits. With the possible exception of Gomul Catena, chains on Callisto do not have recognizable ejecta patterns, but ejecta is generally difficult to identify on this dark, heavily cratered satellite. With few exceptions, Voyager images do not reveal herringbone ejecta or other unusual morphologies (e.g., Oberbeck and Morrison 1974) that might be related to nearly simultaneous adjacent impacts.

It is not possible to directly measure catena crater depths on Callisto due to resolution limits and lack of shadows. Poleward of ±30° latitude, pole-facing slopes on Callisto are covered in bright frosts (Spencer and Maloney 1984), making photoclinometric slope determination techniques

TABLE I
Crater Chains on Callisto and Ganymede: General Characteristics

Crater chain	Chain center Lat.	Chain center Lon.	Length (km)	Azimuth (°)	Colatitude (°)	No. of craters	Spacing (km)	Best image FDS	Best image Res. (km/px)
					Callisto				
a Gomul Catena	34.4	46.8	324	−64.2	77	25	13.5 (±3.3)	16422.25	1.5
b Gipul Catena	67.9	57.1	625	69.7	57	18	36.7 (±10.8)	16428.19	1.3
c Fimbulthul Cat.	8.4	65.4	378	61.9	73	10	42.0 (±8.9)	16422.11	1.6
d Geirvimul Catena	49.2	348.1	90	−88.5	75	6	18.0 (±1.6)	16426.10	1.0
e Eikin Catena	−8.5	15.9	191	−39.7	18	12	19.9 (±10.2)	16421.33	1.7
f Sid Catena	48.7	105.4	78	−12.8	89	7	12.9 (±6.4)	16425.08	1.0
g Gunntro Catena	−19.3	343.3	136	−80.4	24	10	15.1 (±4.4)	16421.18	1.8
h Svol Catena	11.0	37.1	140	45.8	52	10	15.6 (±2.6)	16421.47	1.7
					Ganymede				
j Enki Catena	39.5	13.2	151	−62.4	61	9	18.9 (±12.6)	16403.00	1.9
k Khnum Catena	33.1	347.9	59	−69.1	61	6	11.8 (±4.6)	16405.28	1.1
l Nanshe Catena	15.8	352.0	59	−15.1	25	6	11.7 (± 2.1)	16405.18	1.1
					Shoemaker–Levy 9				
S–L9	—	—	350	—	—	≥13	24.8 (±8.2)	—	—
Mean			202	55.4	56	11	21.9		
STD			(±175)	(±23)	(±24)	(±7)	(±12.9)		

Note. Letter designations (a–l) are keyed to the images in Fig. 1. Catenae names have been approved by the IAU. Catenae on Callisto are named after Norse rivers; on Ganymede, Enki is named after the Babylonian god of the liquid elements, Khnum after the Egyptian watcher of the Nile sources, and Nanshe after the daughter of Enki. Locations based on USGS Misc. Invest. Series I-2035, Controlled Photomosaic of Callisto. Azimuth of crater chains given in degrees clockwise from due north. Colatitude is the degree of curvature of each chain, given as the angle between a point on the chain and best-fit center of curvature of the chain, through the center of the satellite (i.e., the curvature), or 90° for a great circle. Spacing is the mean distance between the centers of adjacent craters. Standard deviations (STD) are given in parentheses. Values for "Shoemaker–Levy 9" are based on a model crater chain formed on Callisto by S–L9, shown in Fig. 13b (see text). The crater for fragment D is neglected because of the overlap with the crater for fragments E and C, and we assume that fragment Q2 was insignificant in comparison to Q1. Means and STD do not include S–L9. Likely secondary crater chains are not included in these tables.

useless. Stereo images of Gipul and Gomul Catenae show, however, that these craters are as deep as typical craters on these satellites (Schenk 1991). The narrow rimwalls and flat floors observed in most catenae craters also indicate that crater depths and morphologies are similar to normal craters in their size range, consistent with an impact origin.

While most catenae craters are approximately circular, a few craters are elliptical, with the long axes of the ellipse always oriented along the direction of the chain. The best examples are seen in Gipul Catena (Fig. 1b), the most prominent chain on either satellite. The most elliptical crater in Gipul Catena has an aspect ratio of ~1.5. One crater near the center of Gipul Catena is split by an arcuate ridge that runs perpendicular to the trend of the chain. Ridges of this type are sometimes observed when two adjacent craters form nearly simultaneously (e.g., Oberbeck and Morrison 1974). The most unusual chain is Nanshe Catena on Ganymede (Fig. 1l). Nanshe Catena is a highly elongated bright ray crater with a scalloped shaped rim. At least six discrete central pits are located on the floor of this crater, aligned along the long axis of the crater and centered between the cusps of the rim scallops. This indicates that Nanshe formed as the result of the nearly simultaneous impact of at least six large distinct projectiles.

Chain Morphology

A total of 116 craters were identified in the 11 crater chains. The number of craters per chain ranges from 6 to 25, with an average of 11 (Table I). Crater diameters range from 3 to 51 km, with a mean of 15.4 km (Table II). Image resolution is 1 to 2 km/pixel, limiting the smallest reliably detectable crater size to ~3 km diameter (only one of the craters is less than 5 km across, which suggests there may not be many undetected small craters). Within each crater chain, crater diameters are roughly similar. The ratio between the diameters of the largest and smallest observed craters in a given chain ranges from 1.4 to ~4, with an average ratio of ~2.2. Spacing between adjacent catena craters is also surprisingly uniform, averaging ~22 km (Fig. 3; Table I). Within the two longest chains, Gipul and Fimbulthul Catenae, spacing varies from 20 to 70 km. In most cases, adjacent crater rims are separated by no more than a few kilometers. In Gomul, Gipul, and especially Geirvimul

FIG. 2. Closeup view of craters in Gomul Catena on Callisto. Despite the modest resolution (~1.5 km/pixel), circular shapes and classic impact crater features, including central peaks, raised rims, and steep rimwalls can be recognized in most craters. Irregularities such as ridges or deviations from circularity are also present in only a few cases, most likely due to interference in nearly simultaneous impact events. Scale bar is 20 km.

Catenae (Figs. 1a, 1b, and 1d), several craters overlap or crosscut adjacent craters by a few kilometers, indicating that the impacts occurred sequentially. This sequence is consistent in all three chains, with the easternmost craters forming first and progressing to the west. Crosscutting relationships are unresolved or do not occur in the other chains.

The lengths of these crater chains range from ~60 to 625 km, averaging ~200 km. It is possible that smaller crater chains have gone undetected due to Voyager resolution limits. For a given imaging system, a feature can be reliably detected if its width is approximately a factor of two greater than the nominal image resolution (e.g., Jensen 1986), in this case 1–2 km/pixel. We should be able to identify crater chains with craters as small as 2–4 km across, and a few linear features with widths of 3.5 to 4 km have been identified on Callisto (Schenk 1995). (These features were classified as endogenic because they occur in parallel sets.) The smallest crater chain has craters averaging 7.4 km across (Table II), well above this threshold, suggesting that there probably is not a large population of small undetected crater chains. High-resolution imaging of these satellites will be necessary to confirm this, however, especially on Ganymede, where very small crater chains might be confused with linear tectonic features.

Catena craters are remarkably aligned (Fig. 1); crater centers exhibit no more than 1 crater radii deviation from a best-fit curve through the craters in each chain. All but one of the chains are slightly curved and lie on small circles, not great circles (Table I). A center of curvature was determined for each chain, using the least-squares methodology of Schenk and McKinnon (1987). The curvature of each chain can be described by its colatitude, defined as the angle subtended from any point on the chain to the center of curvature, through the center of the satellite. The crater chains have an average colatitude of 55° (Table 1).

All of these prominent crater chains on Callisto and Ganymede occur on or within 15° of the Jupiter-facing hemisphere (Fig. 4). Other than this, there is no obvious concentration of crater chains in a given area on the surfaces of these satellites. Also, there is no preferred orientation of these chains on the surface (Table I).

All the prominent crater chains on both Ganymede and Callisto are superposed on preexisting structures or other craters, suggesting that they formed toward the end of the so-called heavy bombardment or later. None are crosscut by younger features. Three of the Callisto chains are superposed on and younger than the Valhalla multiring impact structure (Figs. 1a, 1c, and 1h), a 4000-km-wide feature that postdates roughly two-thirds of all craters on Callisto (Passey and Shoemaker 1982). All three chains on Ganymede post-date bright terrain formation, which covers roughly half of Ganymede's surface. Enki Catena crosses the boundary between bright and dark terrain (Fig. 1j). The major reduction in brightness of the bright ray system of Enki Catena where it crosses into dark terrain illustrates the greater difficulty in identifying ejecta on dark Callisto. On Ganymede and Callisto, stratigraphic age can be crudely determined by the state of preservation of rim morphology, and the fading of crater rim and ejecta brightness with time. Based on these criteria, a wide range of relative ages is apparent for these crater chains, but it is not yet possible to estimate ages for specific crater chains.

ORIGIN OF CRATER CHAINS

Crater chains of various types have been observed on most of the planets and many of the satellites, and are

TABLE II
Crater Chains on Callisto and Ganymede: Fragment and Parent Body Characteristics

	Craters		Fragments		Parent body	
Chain	Diameter (km)	Range (km)	Mass (g)	Diameter (km)	Mass (g)	Diameter (km)
			Callisto			
a Gomul Catena	14.1 (±3.1)	9.9 – 20.1	3.42e + 14 (±2.5e + 14)	0.82 (±0.20)	8.55e + 15	2.54
b Gipul Catena	28.8 (±6.4)	19.1 – 37.0	1.56e + 16 (±1.0e + 16)	2.94 (±0.74)	2.81e + 17	8.12
c Fimbulthul Cat.	11.9 (±2.5)	6.1 – 14.8	1.60e + 14 (±8.3e + 14)	0.64 (±0.14)	1.60e + 15	1.46
d Geirvimul Cat.	19.5 (±3.0)	16.6 – 24.3	2.41e + 15 (±1.3e + 15)	1.62 (±0.28)	1.45e + 16	3.02
e Eiken Catena	8.0 (±2.3)	5.8 – 11.5	4.14e + 13 (±3.8e + 13)	0.40 (±0.12)	4.97e + 14	0.98
f Sid Catena	8.7 (±1.9)	6.7 – 12.5	5.48e + 14 (±4.9e + 14)	0.96 (±0.24)	3.84e + 15	1.94
g Gunntro Catena	11.8 (±3.6)	6.6 – 17.2	3.15e + 13 (±4.0e + 13)	0.34 (±0.14)	3.15e + 14	0.84
h Svol Catena	7.4 (±2.4)	4.9 – 12.6	3.44e + 14 (±3.2e + 14)	0.78 (±0.28)	3.44e + 15	1.88
			Ganymede			
j Enki Catena	16.5 (±1.8)	14.5 – 19.9	4.61e + 14 (±1.8e + 14)	0.94 (±0.12)	4.15e + 15	1.00
k Khnum Catena	9.9 (±4.5)	3.3 – 14.6	1.91e + 14 (±1.9e + 14)	0.60 (±0.30)	1.14e + 15	0.65
l Nanshe Catena	44.2 (±5.1)	38.3 – 50.9	1.47e + 16 (±5.9e + 15)	3.00 (±0.40)	8.86e + 16	2.76
			Shoemaker–Levy 9			
S–L9	22.7 (±6.3)	12.5 – 31.6	—	—	—	~1.5–2.0
Median			3.0e + 14		3.8e + 15	
Mean	15.4 (±8.8)		3.4e + 15 (±7.3e + 15)	1.2 (±0.8)	3.7e + 16	2.7
STD					(±8.5e + 16)	(±2.2)

Note. Mean fragment masses and diameters are based on crater sizes and scaling arguments (McKinnon and Schenk 1995). Parent body masses are obtained by summing fragment masses. Effective diameters in both cases are computed assuming a sphere of density 1.0 g/cm^3. Standard deviations (STD) are given in parentheses. Values for "Shoemaker–Levy 9" are based on a model crater chain formed on Callisto by S–L9, shown in Fig. 13b (see text). The crater for fragment D is neglected because of the overlap with the crater for fragments E and C, and we assume that fragment Q2 was insignificant in comparison to Q1. Means, medians, and STD do not include S–L9. S–L9 diameter estimates are from Scotti and Melosh (1993) and Asphaug and Benz (1996).

either impact related or endogenic. Pit chains associated with grooves on Phobos might have been formed by regolith drainage into internal fractures (Thomas 1979). Chains of pits are common in volcanic provinces or associated with extensional structures on Earth, Mars, the Moon, and even on Triton (Croft *et al.* 1995). Endogenic crater chains are most easily recognized by their wide range of morphologies and by their spatial association with endogenic geologic features. Callisto is noted for a virtual lack of endogenic geologic activity, except for very rare and mostly very ancient fracture sets and (possible) volcanic deposits (e.g., McKinnon and Parmentier 1986, Schenk 1995). Linear endogenic features abound on Ganymede, but no concurrent volcanic deposits or structural features of any type are observed in association with the prominent crater chains on Ganymede or Callisto (Fig. 1). It is most unlikely that the craters in these chains are the result of endogenic (especially volcanic) activity on either satellite. The formation of central peaks, raised rims, and ejecta patterns is most consistent with an impact origin for these crater chains on both satellites (Passey and Shoemaker 1982).

Secondary Crater Chains on Callisto and Ganymede

Passey and Shoemaker (1982), in their post-Voyager survey of cratering on Ganymede and Callisto, proposed that crater chains on Callisto formed as a result of the impact of strings of secondary fragments ejected from Valhalla or other large, unseen, basins. This was based on the apparent similarity of the crater chains on Callisto to secondary chains on the Moon and on the lack of an alternative origin. In this section we reevaluate the morphology and distribution of the prominent crater chains on Ganymede and Callisto and show they are probably not the result of secondary cratering.

Secondary crater chains (Figs. 5a, 5b) are common on the Moon (e.g., Schultz 1976, Wilhelms 1987) and Mercury (e.g., Gault *et al.* 1975). Obvious secondary crater chains are less common on the icy satellites, but several chains are observed surrounding at least two large basins on Ganymede, Gilgamesh, and the "Western Equatorial Basin" (Figs. 5c, 5d, and 5e). Like those observed on the Moon and Mercury, secondary crater chains on the Galilean satellites have distinct morphologic properties. Cra-

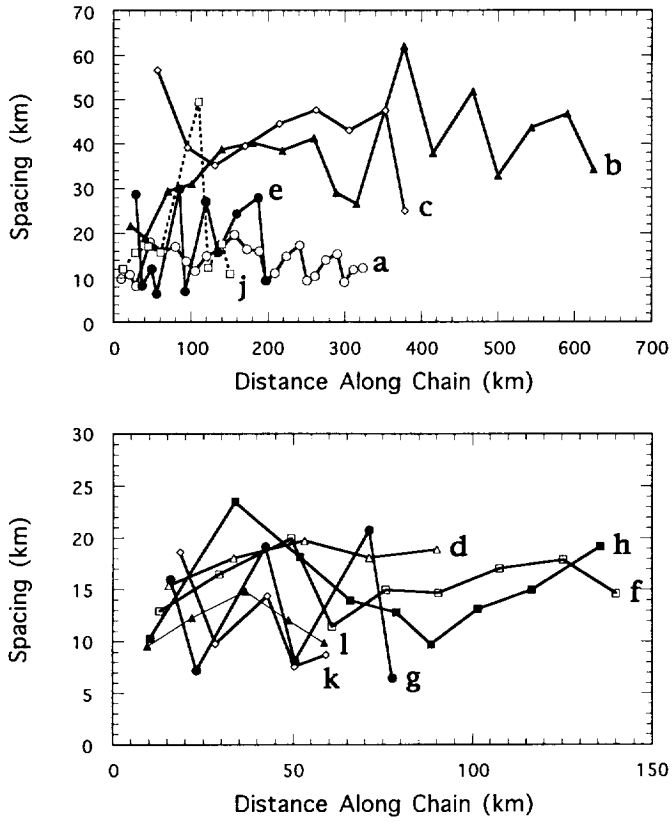

FIG. 3. Spacing of craters within crater chains. Spacing is given as the distance between the centers of adjacent craters, plotted at the midpoint between craters. Each chain is labeled (see list in Table I). Data are split into two figures, with different scales, for clarity. Errors are ~3 km. Chains f and g are not plotted due to poor image quality.

ters in secondary chains can be roughly circular to irregular in shape (Fig. 5). Secondary chains are usually associated with other secondary craters in a broad zone concentric to the source crater and just beyond the continuous ejecta blanket (e.g., Figs. 5b, 5c, 5e, and 5g), but can occur as isolated features up to a few thousand kilometers from the basin center (Figs. 5a, 5d). Within secondary chains, craters can overlap or crosscut adjacent craters. When this is well expressed, the craters are inferred to have formed sequentially outward, with the craters closest to the source basin forming first (Figs. 5a, 5e, and 5g). This occurs because ejecta launched to greater distances fall later and form craters that crosscut those just formed by ejecta launched to shorter distances.

Secondary crater chains on the Moon (Fig. 5a) and on Mercury (Fig. 5b) are usually oriented radially to the source basin. Three crater chains on the lunar farside, Catenae Artamonov, Gregory, and Dziewulski, are radial to the center of the 900-km Imbrium basin (Fig. 6; e.g., Wilhelms 1987), even though they are ≥3000 km from Imbrium center. Catena Mendeleev is radial to Tsiolkovskiy (D = 180 km; Fig. 6, Wilhelms 1987). The Davy crate chain is also radial to Orientale, and Catena Sumner may be radial to Serenitatis or Humorum (Fig. 6). A prominent secondary chain north of Copernicus on the Moon is an exception to this rule, but that chain is close to the primary crater and craters within it have very irregular shapes. A complete survey of lunar and mercurian crater chains is beyond the scope of this report, but prominent examples on the Moon (and Ganymede) support the conclusion that secondary chains are radial to their source basin (especially when not proximal to it) and craters within them overlap in sequence outward from the basin.

Only a few features on Callisto appear to be secondary crater chains. A ~400-km long linear feature at 20°N, 30°W is located within the eastern portion of the Valhalla multiring basin (Fig. 5g). This feature is radial to the center of Valhalla (Fig. 7a) and consists of approximately 20 small craters of variable size and morphology. In several cases, the "craters" have a groove-like morphology. This feature is discontinuous, with gaps of up to 100 km, and its apparent relative age (based on rim brightness) is similar to those of Valhalla structures and secondaries nearby and at similar distances from the center of the basin. We conclude that this linear feature is either a secondary crater chain or a radial tectonic feature associated with the formation Valhalla.

A crater chain north of Valhalla, at 50°N, 73°W, consists of three equidimensional craters ~12 km across (Fig. 5h). This chain is approximately radial to the center of Valhalla (Fig. 7a) and is situated within a field of secondary craters due north of Valhalla. The three craters overlap sequentially outward, indicating that the impacts progressed outward from Valhalla, as expected for secondary crater chains. The apparent relative age of this chain is also roughly similar to those of nearby Valhalla structures and secondaries. We conclude that this feature is a secondary crater chain formed by Valhalla. A crater chain located on the anti-jovian hemisphere at 22°S, 185°W consists of three to four craters (Fig. 5). The largest crater is irregular in shape with a large irregular mound in the center, more consistent with a secondary or grazing impactor. The high density of similar appearing craters in this area suggests that the alignment of these craters may be coincidence.

We examine two lines of evidence against a secondary cratering origin for the other prominent crater chains identified here (Fig. 1): the scarcity of large potential source craters or basins, and the lack of alignment of these chains with these few large impact craters. The mean diameter of the largest secondary craters (D_2) scales with the diameter (D_p) of the associated primary crater on the Moon (Allen 1979), $D_2 \sim 0.14 D_p^{0.77}$, providing lower bounds on the sizes of potential source basins. The relation for craters on Ganymede and Callisto is very similar (S. Croft, personal communication 1987) but less well documented and we

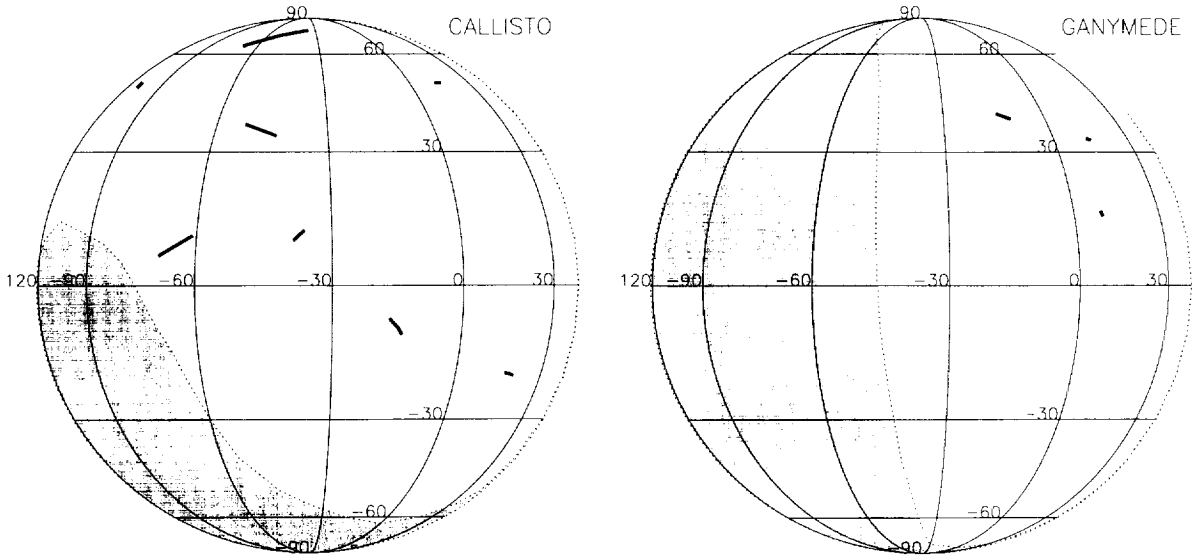

FIG. 4. Orthographic views of Callisto and Ganymede centered on the average trajectory vectors for disrupted comets showing the observed crater chains (solid heavy lines). These hemispheres are subject to impact from outgoing comets disrupted by Jupiter. Areas viewed at low resolution are highlighted by stiples (dotted curves). Disrupted comet impact scars are not expected on the opposite hemisphere, consistent with observation. (Figure modified from McKinnon and Schenk 1995.)

use the lunar relationship. The average crater diameter within chains on Callisto and Ganymede ranges from ~7 to ~40 km. If any of these chains are secondaries, then they would likely originate from primary basins ~175 to ~1750 km across (the average chain would require a source basin at least 450 km across). The only craters or basins larger than ~175 km across identified on Callisto are the giant Valhalla multiring basin (crater diameter ~1000 km, Schenk 1995), and possibly the Asgard multiring basin, the large bright crater Adlinda, and two penepalimpsests near Adlinda and Asgard (crater rim diameters unknown). The only large basins on Ganymede are the penepalimpsests Ilus and Nidaba, an unnamed basin (at 23°N, 181°W), the Western Equatorial Basin, (all between 175 and 210 km across), and the Gilgamesh multiring basin ($D_p \sim 575$ km). Examination of low-resolution images (~10 km/pxl) of the ~20% of the surface of either satellite poorly imaged by Voyager does not reveal any obvious indication of additional sufficiently large impact structures, although this conclusion is subject to new Galileo images.

Passey and Shoemaker (1982) suggested that the source basin(s) for some of these chains have disappeared as a

FIG. 5. Secondary crater chains on planets and satellites. (a) Catena Dziewulski, a secondary crater chain ~70 km long on the lunar farside. This chain and two similar nearby chains, Catenae Gregory and Artamonov, are radial to the Imbrium basin (direction of large arrow), even though they are ≥3000 km distant. Groove adjacent to crater chain is also radial to Imbrium. Small arrows indicate overlap of adjacent craters. The overlap indicates that the impacts occurred in sequence from north (top) to south, consistent with an origin by secondary impact from Imbrium. Location of chain is shown in Fig. 6. Oblique image (Apollo 16 frame M-3009, see also AS12-55-8201) has not been rectified. (b) Secondary crater chains on Mercury radial the nearby basins. Image is orthographic projection of Mariner 10 frame 154, centered on 60°N, 134°W. Scale bar is 50 km. (c) Secondary crater chain on Ganymede (arrow), radial to the 175-km diameter Western Equatorial Basin (upper right). Voyager PICNO 0479J2-001. Scale bar is 50 km. (d) Secondary crater chain on Ganymede, at 3°S, 127°W. This irregularly shaped chain is radial to the 575-km diameter Gilgamesh basin, located 3000 km due south (arrow) and shown in (e). Location and great circle trace shown in Fig. 7c. Scale bar is 50 km. Image is orthographic projection of PICNO 0467J2-001 at 0.9 km/pixel resolution. (e) Secondary crater chains on Ganymede radial to the 575-km diameter Gilgamesh multiring basin. Many craters are irregular in shape. Overlapping craters are also apparent (small arrows). Smooth region at top of image is part of the continuous ejecta deposit. Orthographic projection is centered on Gilgamesh (direction of large arrows). Scale bar is 50 km. (f) Crater chain on Callisto (20°N, 30°W). Outer rings associated with the Valhalla multiring impact structure are visible throughout. Chain is radial to and interpreted as a secondary crater chain (or tectonic feature) associated with the Valhalla basin (direction of large arrow). Chain location is shown in Fig. 7a. Image is orthographic projection of PICNO 0164J1+000 at 0.9 km/pixel resolution. (g) Crater chain on Callisto (50°N, 73°W). Chain is radial to and interpreted as a secondary crater chain associated with the Valhalla basin (direction of large arrow). Chain location is shown in Fig. 7a. Image is orthographic projection of PICNO 0327J1+000 at 0.9 km/pixel resolution. (h) Possible secondary crater chain on Callisto located at 22°S, 185°W. Chain location is shown in Fig. 7a. Voyager image 0430J2-002 with resolution of ~7 km/pixel.


a

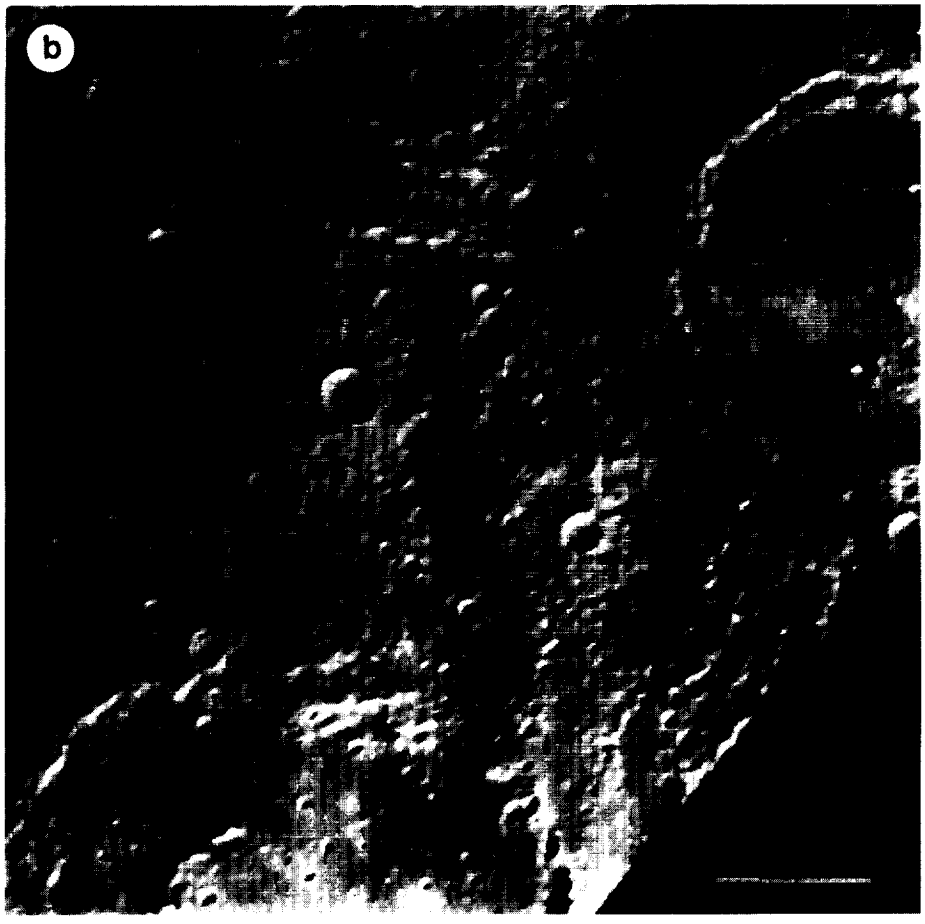
b

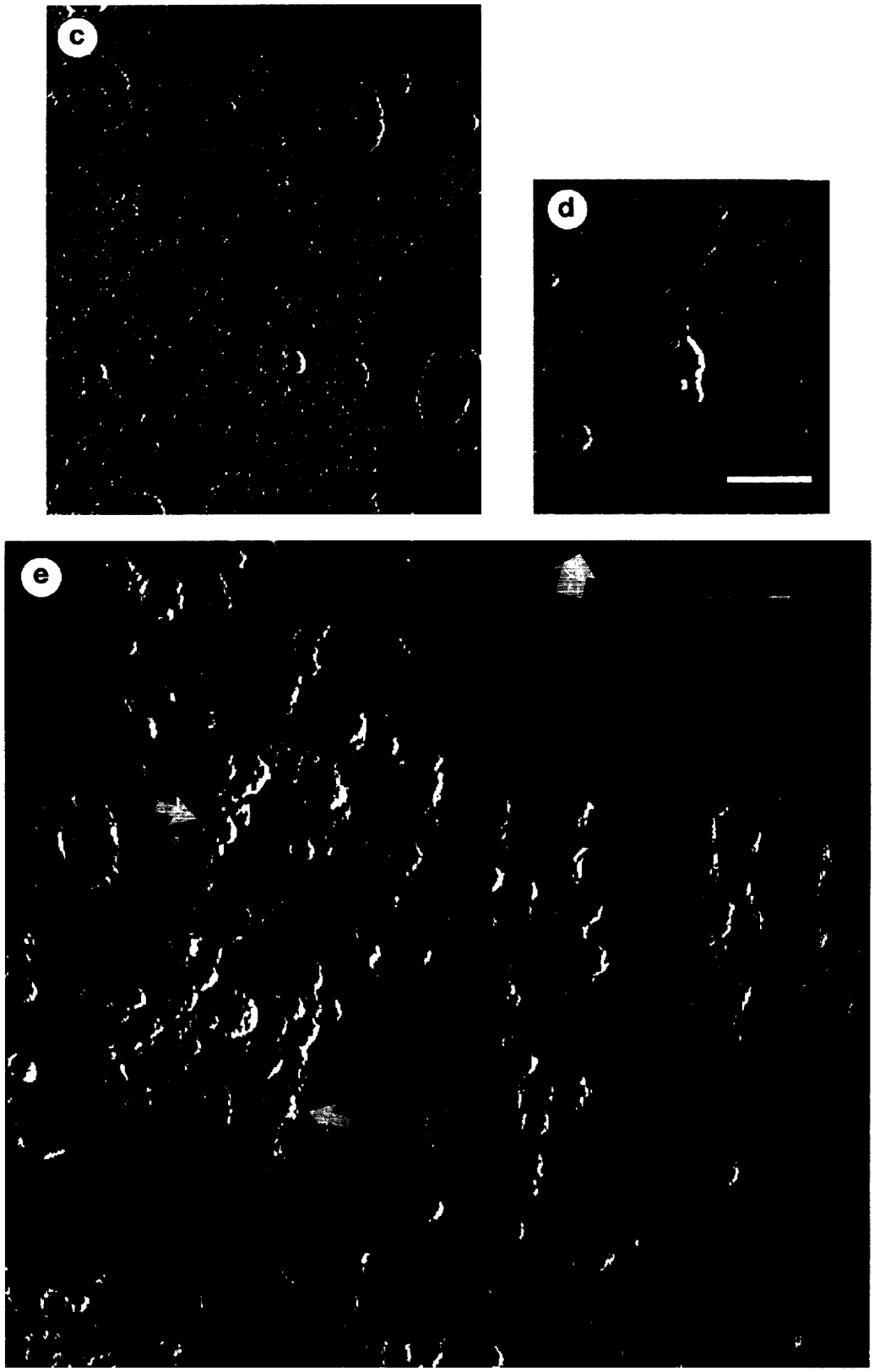

FIG. 5—*Continued*

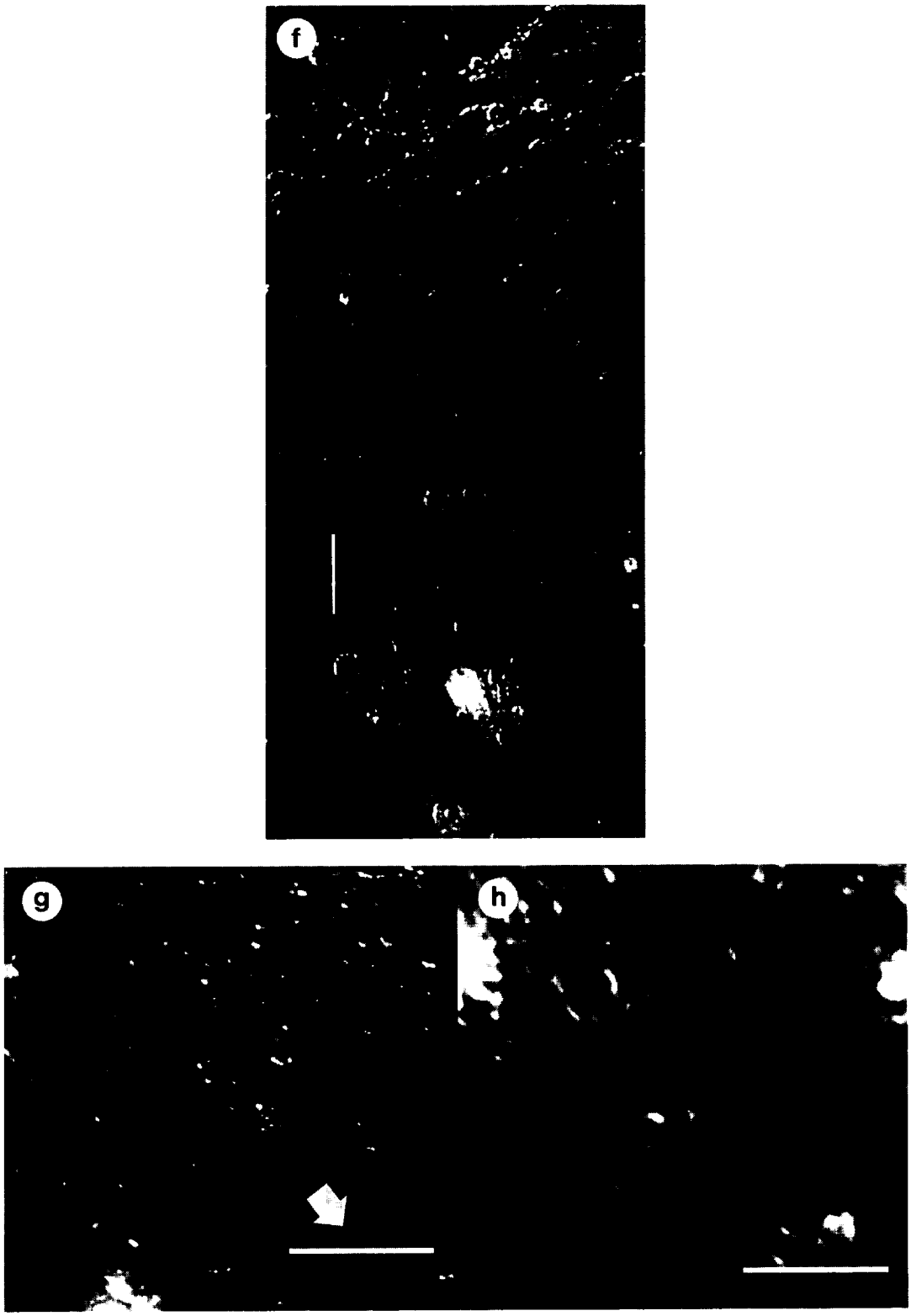

FIG. 5—*Continued*

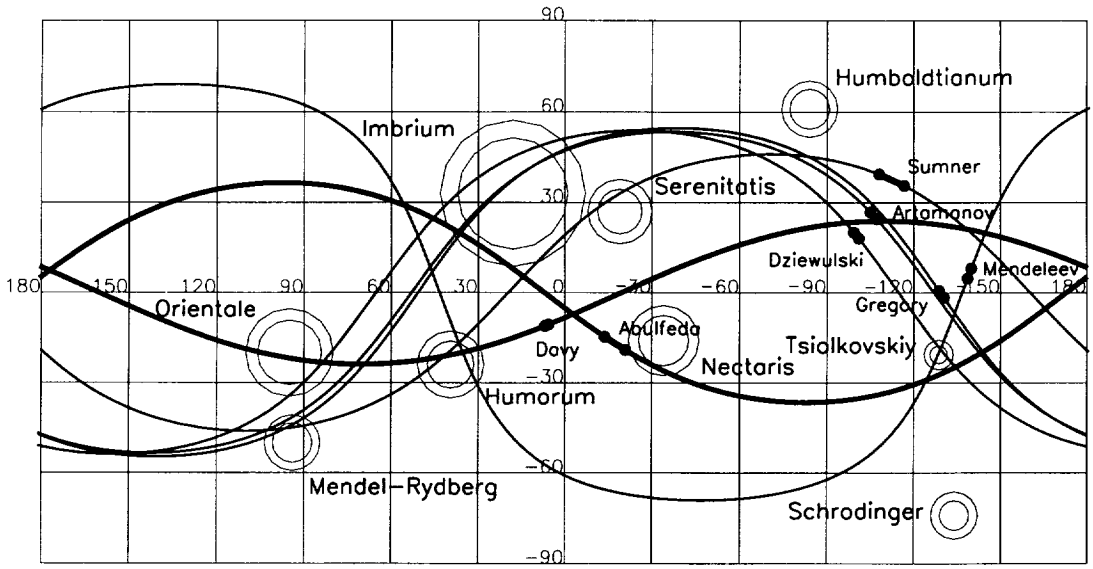

FIG. 6. Cylindrical map of the Moon, showing large impact structures (concentric circles), locations of prominent crater chains (filled circles), and great circle fits to chain endpoints (solid curves). Basins are shown approximately to scale. Artamonov, Dziewulski (Fig. 5a), and Gregory are radial to Imbrium, Mendeleev is radial to Tsiolkovskiy, and Sumner may be radial to Humorum or Serenitatis. Davy and Abulfeda chains (heavy curved lines) have been proposed to be due to impact of split comets (Melosh and Whitaker 1994, Wichman and Wood 1995). The orientation of Davy radial to Orientale and the rough similarity in ages (both post-Imbrium, e.g., Wilhelms 1987) suggest that Davy may be a secondary crater chain (a question that is a subject for future consideration). The great circle trace of Abulfeda passes near Imbrium, but this chain is ~30° to the trend of Imbrium sculpture in this area and has no obvious source basin.

result of viscous relaxation. The relative youth and morphological freshness of the crater chains (above) makes it highly unlikely that impact basins at least a few hundred kilometers across with ages similar to or younger than Valhalla or Asgard could have "disappeared." Crater palimpsests may have relaxed viscously leaving little topographic expression, although they do leave a circular high albedo remnant. They are, however, older than bright terrain on Ganymede, and are degraded and stratigraphically very old on Callisto as well (e.g., Passey and Shoemaker 1982). Palimpsests are thus too old to be source basins for any of these crater chains.

To search for links to any of the possible source basins (seen or unseen), we fit great circles to the endpoints of the identified crater chains and compare these traces to the locations of these potential source craters (Fig. 7b), as we did for the Moon (Fig. 6). Even though small circles are better fits to chain shape (above), for this source basin search we assume great circles based on the tendency for distal crater chains to be radial to their source basin (Figs. 5, 6). Four chains (Fimbulthul, Eikin, Gunntro, and Geirvimul Catenae) have great circle traces that are approximately radial to or pass through part of the large Valhalla basin (Fig. 7b). The large size of Valhalla increases the random probability that at least some of these chains will have traces that pass near the basin. Although radial to Valhalla, Fimbulthul Catena (Fig. 1c) is clearly superposed on the ring structure and the ejecta blanket of this basin and is thus younger than Valhalla. Craters in Eikin Catena (Fig. 1e) are relatively bright compared to Valhalla structures and the two Valhalla secondary chains described above (Fig. 5). We conclude that this chain is probably younger than Valhalla. The relative ages of Geirvimul and Gunntro Catenae are less clear. Gunntro Catena (Fig. 1g) is ~3000 km from the center of Valhalla, considerably further than the secondary crater chains that have been identified (Fig. 5). A link to Valhalla is considered unlikely but cannot be conclusively ruled out. The craters in Geirvimul Catena (Fig. 1d) overlap from east to west, indicating that the craters nearer to Valhalla formed last (Fig. 1d). This is contrary to the observation that craters in secondary chains nearer to the source basin form first. We conclude that this chain is probably not related to Valhalla. The great circle trace of Gomul Catena passes near the Asgard basin. This chain is superposed on Valhalla, which is estimated to be younger than Asgard (Passey and Shoemaker 1982). If so, Gomul Catena must also be younger than Asgard. In addition, no other candidate basins on Callisto are likely to be the source craters for any of these chains (Fig. 7b).

On Ganymede, the great circle trace of the oldest chain, Khnum Catena (Fig. 1k), is radial to the 140-km bright-rayed central dome crater Punt Facula. Khnum Catena lacks bright ejecta deposits and is too old to be associated with Punt. The great circle trace of Khnum Catena is also

radial to the "Western Equatorial Basin." Khnum is roughly 6000 km distant from both this basin and Punt, however, and a relationship to either basin is unlikely because of this great distance. The large bright-rayed crater chains on Ganymede, Enki, and Nanshe Catenae (Figs. 1j, 1l), are also too large and too young to have been formed by any known or likely impact basins on Ganymede identified above, including Nidaba (Fig. 7c), all of which lack bright rays and are too old. The sizes of craters in Enki and Nanshe Catenae imply source basins at least 500 and 2000 km in diameter, respectively. Neither of these chains have great circle traces that pass even close to Gilgamesh ($D \sim$ 575 km), the largest impact structure known on Ganymede.

Halfen *et al.* (1990) suggested that very low angle (<15°) impactors striking a given satellite could produce linear strings of ricochet fragments that would escape and potentially strike another satellite. Statistically, less than 10% of all impacts could potentially produce this effect, and then only for larger impacts capable of launching kilometer-sized fragments (Halfen *et al.* 1990). Very few such ricochet fragments would strike another satellite; most would escape Jupiter's gravity or disperse before striking a satellite. If all catena on the satellites are formed from this process, then a ricochet event could be expected to occur in the jovian system once every few 100 years or so, based on the likely age of these surfaces and the observed occurrence of crater chains (see Frequency of Tidal Disruption Events in the Jupiter System below). If so, then to produce enough ricochet fragments out of the total impact population to produce crater chains (for every putative ricochet event there is a factor of at least 10 additional "normal" cratering events), a large impact event must be occurring every few tens of years among the Galilean satellites, an unlikely scenario considering the observed cratering record. Also, the geometric cross-sections that ricochet fragments must travel through are substantially smaller than those appropriate to disrupted comets (McKinnon and Schenk 1995).

The unusual dimensions of these crater chains, lack of suitable source basins, lack of geologic activity on Callisto, and improbability of impact of ricochet fragments, all indicate that the impacts of secondaries from large basins are unlikely to have formed most of the crater chains described here. Because of the lack of suitable source basins for the 11 prominent crater chains identified on Callisto and Ganymede (Table I), we henceforth refer to them as "anomalous" crater chains.

Formation of Crater Chains by Tidally Disrupted Comets

The linear "string of pearls" comet Shoemaker–Levy 9 was the first disrupted comet to be observed shortly after breakup due to tidal forces, in this case during a close pass by the planet Jupiter. This comet train consisted of up to 21 individual fragments roughly similar in apparent size, roughly equally spaced, and arrayed linearly in space. These characteristics are very similar to those of the anomalous crater chains on Callisto and Ganymede described above. Melosh and Schenk (1993) used a simple tidal evolution model to show that similar tidally disrupted comets on the order of 1 km across would produce fragment chains a few hundred kilometers long if they struck Ganymede and Callisto, consistent with the observed lengths of crater chains. Asphaug and Benz (1994) reached a similar conclusion from their modeling of tidal disruption.

Melosh and Schenk (1993) concluded that disrupted comets must form crater chains on the jovian satellites on the initial outbound orbit following disruption; otherwise, the fragment chains become too dispersed to produce the chains observed on these satellites if the comet train returns to Jupiter, as demonstrated by S–L9. McKinnon and Schenk (1995) investigated the encounter geometries of disrupted comets in the Jupiter system. Outbound comet trajectories are approximately radial to Jupiter. Mean angles between outgoing comet trajectory vectors and the radius vector to Jupiter are relatively small (~13° and ~18° for Callisto and Ganymede, respectively). With the velocities of outgoing comets and satellite motion taken into account, the "target hemisphere" subject to impact from outgoing disrupted comets shifts westward onto the leading hemisphere by ~35° of longitude (Fig. 4, McKinnon and Schenk 1995). All the anomalous crater chains occur in these hemispheres (similar Voyager imaging coverage and resolution exists on both hemispheres). The detailed morphological characteristics of anomalous crater chains on these satellites indicate that the impact of tidally disrupted comets is most probably the only viable explanation for most of the crater chains on these satellites.

ANOMALOUS CRATER CHAINS IN OTHER PLANET–SATELLITE SYSTEMS

Following the discovery of S–L9 and the proposal by Melosh and Schenk that crater chains on the jovian satellites are due to disrupted comets, it became apparent that this process could occur elsewhere in the Solar System. A disrupted comet origin has been proposed for two unusual crater chains on the near side of the Moon, where Earth would be responsible for disruption (Melosh and Whitaker 1994, Wichman and Wood 1995). Sungrazing comets frequently break up near solar perihelion (e.g, Marsden 1989), and Mercury might be a target for such objects. We have applied the general tidal splitting model of Melosh and Schenk (1993) in order to predict the lengths of crater chains on other planets and satellites (Table III). For a 2-km diameter comet passing within 1.5 solar radius of the Sun, we expect a comet chain length of ~1500 km at Mercury, and a chain length of ~15,000 km for a 20-km diameter comet. Disruption of sungrazing comets may also be

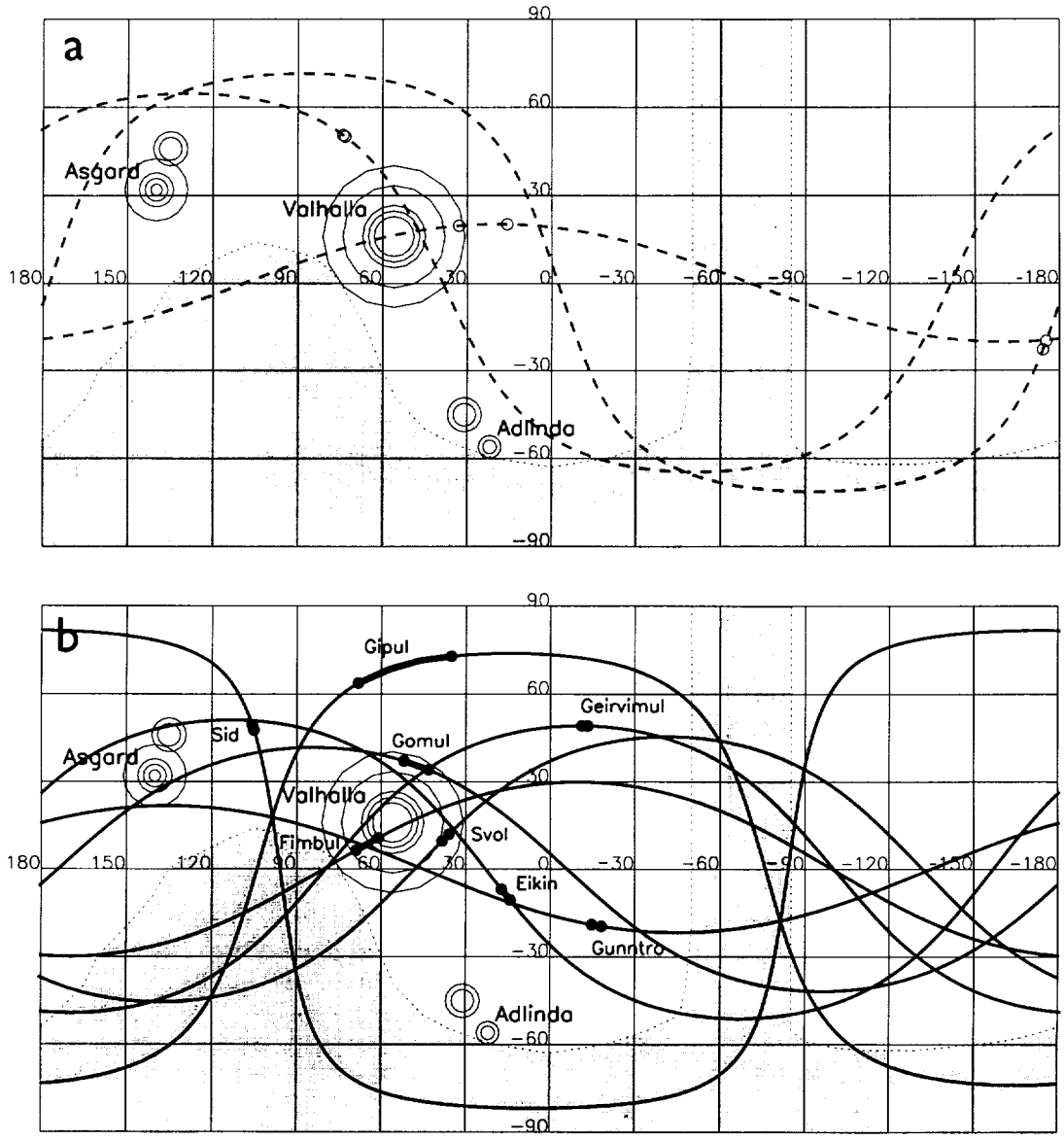

FIG. 7. Cylindrical maps of (a, b) Callisto and (c) Ganymede, showing large impact structures (concentric circles), locations of prominent crater chains (filled circles), and great circle fits to chain endpoints (solid curves). Also shown are known secondary crater chains (dashed curves), described in text and shown in Fig. 5. Areas viewed at low resolution are highlighted by stiples and dotted curves. Basins are shown approximately to scale. For a 60 km long chain on Callisto, an error of ~0.1° (±4 km) in the position of an endpoint translates into an error of ~4° in the great circle position 90° from the chain location. This error is considerably smaller for longer chains and is negligible compared to the size of the basins in question.

influenced by nontidal forces, however, such as from outgassing due to intense heating, resulting in nonlinear dispersed clusters (e.g., Sekanina 1982). In any case, no linear comet trains have been observed near the Sun, and no linear crater chains have been recognized on Mercury, except those associated with obvious secondary crater fields (Fig. 5b, Gault *et al.* 1975).

The other giant planets, particularly Saturn, are potential sites for formation of disrupted comet crater chains, due to their high gravitational potential and numerous satellites. Application of the Melosh and Schenk tidal model predicts that crater chains would be visible on satellites of the outer planets (Table III), if comet disruption occurs within these satellite systems. Comet chains on the inner saturnian satellites may be too short to produce true crater chains in some cases, depending on encounter scenarios (Table III). Only a few putative "crater chains" have been observed on these small satellites. The best example is Pu Chou Chasma, a degraded >500-km-long trough-like structure on Rhea. This feature runs parallel to at least one other

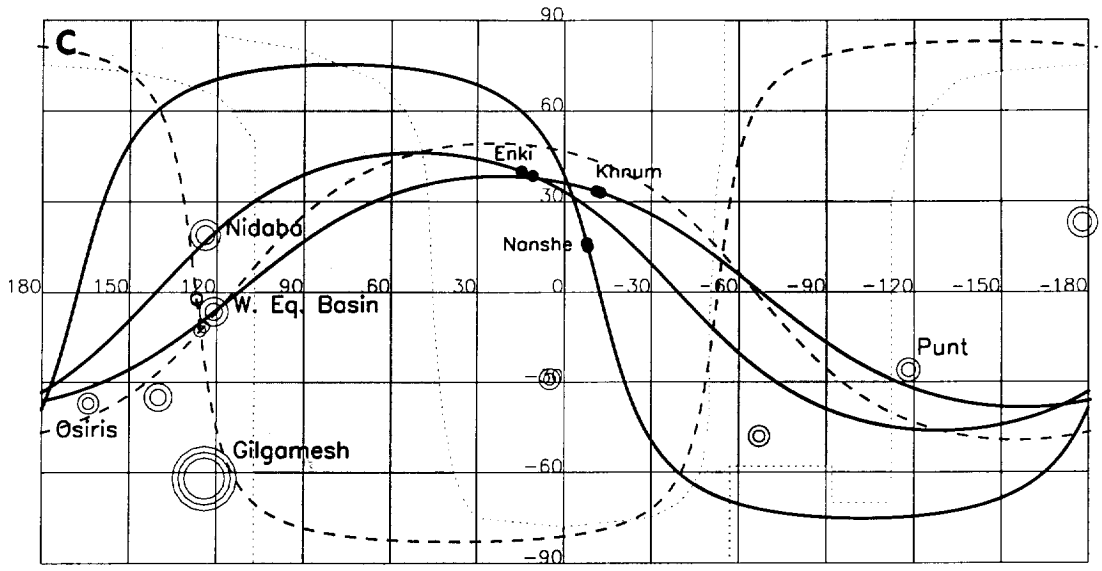

FIG. 7—*Continued*

TABLE III
Predicted Lengths of Crater Chains on the Outer Satellites

	Crater chain lengths (km)		
r_{min}/R_p	(v_∞ = 0.01 km/s)	(v_∞ = 5 km/s)	(v_∞ = 10 km/s)
	Enceladus		
1.0	16	15	13
1.5	9	8	7
2.0	6	5	5
2.5	4	4	3
	Rhea		
1.0	56	51	40
1.5	29	26	20
2.0	19	17	13
2.5	13	12	9
	Titan		
1.0	234	194	132
1.5	116	96	64
2.0	72	58	39
2.5	50	40	26
	(v_∞ = 0.01 km/s)	(v_∞ = 1 km/s)	(v_∞ = 5 km/s)
	Triton		
1.0	128	126	95
1.5	65	64	47
2.0	40	40	29
2.5	28	28	20

Note. Calculations for a given perigee distance (r_{min}) and planetary diameter ($2R_p$) based on a comet 2 km wide with an approach velocity of v_∞ (Melosh and Schenk 1993).

groove-like structure, suggesting that both are probably of internal origin (Moore *et al.* 1985). Several crater or pit chains have been mapped on Dione (Moore 1984) and Enceladus (Kargel and Pozio 1996), but in each case, the geologic association of these chains with other linear features favors an endogenic origin. A chain of three aligned craters, 2–3 km across, has been identified on Triton (22°N, 15°E). This feature is located in a geologically complex region, and an impact origin is uncertain. There thus appears to be no clear record of impact of disrupted comets in any of the other satellite systems. A search for chains on cloud-covered Titan (which is similar in size to Callisto and may have an extensive cratering record) must await the arrival of the Cassini orbiter in 2007.

As discussed by Asphaug and Benz (1996), however, S–L9-type disruption events may be impossible at Saturn because comets would have to have periapses inside the planet (because of its low density) in order to experience sufficient tidal stress to break up. Jupiter's large gravitational cross-section and smaller distance from the Sun (as compared with the other giant planets) result in a higher rate of encounters with short-period comets. Many of these comets have aphelia of their orbits near Jupiter's orbit, resulting in frequent low-velocity encounters. In addition, the larger sizes of the galilean satellites and the higher velocity of comets passing through Jupiter's gravitational field all favor the formation and retention of disrupted comet crater chains at Jupiter, consistent with the geologic record. The effects of this on cometary populations and projectile fluxes in the Jupiter region may be significant and are subjects for future consideration.

FREQUENCY OF TIDAL DISRUPTION EVENTS IN THE JUPITER SYSTEM

Crater chains on the galilean satellites provide the only available record of ancient cometary disruption events in the jovian system. Given the small relative cross-sections of these satellites as seen from Jupiter, very few comets leaving the Jupiter system will actually strike the satellites. Most will escape and a very few might be devoured by Jupiter on subsequent orbits if the disrupted comet was in temporary orbit like S–L9 (e.g., Benner and McKinnon 1995). The percentage of comets disrupted by Jupiter that have struck a given satellite is given approximately by the ratio of the projected area of the disc of the satellite (of radius R) to the potential surface area represented by the sphere of its orbit (with semi-major axis r). Gravitational focusing by the satellites is negligible, amounting to a 2% increase in cratering rates (McKinnon and Schenk 1995). The frequency, ν, of comet disruption events is then related to the observed number of chains, N, corrected for the percent of the target hemisphere actually observed by Voyager at resolution suitable for recognition of crater chains, f (~80% and ~57% for Callisto and Ganymede, respectively), the above ratio, and the age of the surface, t

$$\nu \simeq 4\pi N r^2 / R^2 f t(\pi + 4v_o/v_c) \quad (1)$$

The form of this equation accounts for the fact that the satellite is sweeping out a volume of space and that the orbital (v_o) and cometary velocities (v_c) are roughly comparable and nonnegligible. Short-period comets travel at ~19.5 and ~15 km/sec as they pass the orbits of Ganymede and Callisto (McKinnon and Schenk 1995), which rotate synchronously with orbital velocities of ~11 and ~8 km/sec, respectively. We assume mean ages (t) of the surface of 4×10^9 and 3.5×10^9 years for Callisto and Ganymede (Shoemaker and Wolfe 1982), respectively.

Averaged over Callisto's geologic history, the estimated frequency at which Jupiter disrupts close-approaching comets based on Eq. (1) is $\sim 3.7 \times 10^{-3}$/year, or one disruption event every ~275 ± 100 years ($\sqrt{n}$ statistics). For comets larger than ~2 km across, of which approximately four struck Callisto (Table 2), this interval is ~550 ± 225 years. Similarly, for Ganymede these values are $\sim 5.8 \times 10^{-4}$/year, or 1 event every 1730 years. Approximately half of Ganymede has been resurfaced by volcanic materials, however, and the surface may be considerably younger than 3.5×10^9 years (Shoemaker 1994). Crater densities for cratered dark terrain on Ganymede are lower than on Callisto by a factor of ~3, and lower by ~3 to 10 for young bright terrain (e.g., Woronow *et al.* 1986). The factor of ~3 lower number of chains on Ganymede is related in part to the less than complete Voyager coverage (Fig. 4), and to the extensive resurfacing, which resulted in a shorter cratering history on Ganymede. The greater difficulty in recognizing chains on Ganymede's tectonically deformed terrains may also bias our sample. We adopt the Callisto values as a more representative sampling, recognizing that cratering and hence disruption rates may have been higher in the distant past.

The estimated frequency of cometary disruption indicates that some 10^7 disruption events have occurred during the period of Callisto's geologic record ($\sim 4 \times 10^9$ years). No impact craters of any kind are observed on Io, due to continuing resurfacing, and no crater chains have been observed on Europa due to poor imaging resolution and the extreme youth of its surface (Lucchitta and Soderblom 1982). Assuming a mean age of $\sim 3 \times 10^7$ years for Europa's surface (Shoemaker 1994), we predict from Eq. (1) and the estimated disruption frequency of $\sim 3.7 \times 10^{-3}$/year that there is only a 3% probability that a single crater chain will be observed globally on Europa by the Galileo Orbiter. Additional crater chains may be discovered in poorly imaged areas of Callisto and Ganymede, particularly Ganymede where 43% of the target hemisphere (between ~40° and 125°W longitude) was seen poorly. We expect at least two to three anomalous crater chains remain to be discovered in this region of Ganymede.

FRAGMENT AND PARENT COMET CHARACTERISTICS

Comet Fragments: Masses and Diameters

Using Schmidt-Holsapple scaling (in the gravity regime), McKinnon and Schenk (1995) estimated the masses of comet fragments that formed catena craters. Scaling of projectile mass is a function of impact geometry and velocity, which are usually unknown for specific craters. The constraint of passage within the Roche limit of Jupiter, together with the known locations of chains on these surfaces, allowed McKinnon and Schenk to estimate these parameters with some confidence, making realistic mass estimates for catenae fragments possible. We note that the overall scaling uncertainty in their fragment masses is approximately a factor of 3.

Estimated masses of individual fragments responsible for each crater range over 4 orders of magnitude, roughly 10^{12}–10^{16} g (Table II, Fig. 4 of McKinnon and Schenk 1995). Within each of the crater chains, however, derived fragment masses are more uniform and are restricted to a range of only ~1 order of magnitude (Table II; McKinnon and Schenk 1995). Thus, fragments of roughly similar mass are produced in each disruption event, but this characteristic mass is different for each event (Table II). Assuming densities of 1 g/cm^3, mean fragment diameters were estimated to be 1.2 ± 0.8 km (Table II). Mass estimates can be corrected for a density of 0.6 g/cm^3 (preferred by Solem (1994) and Asphaug and Benz (1994) for a nonrotating

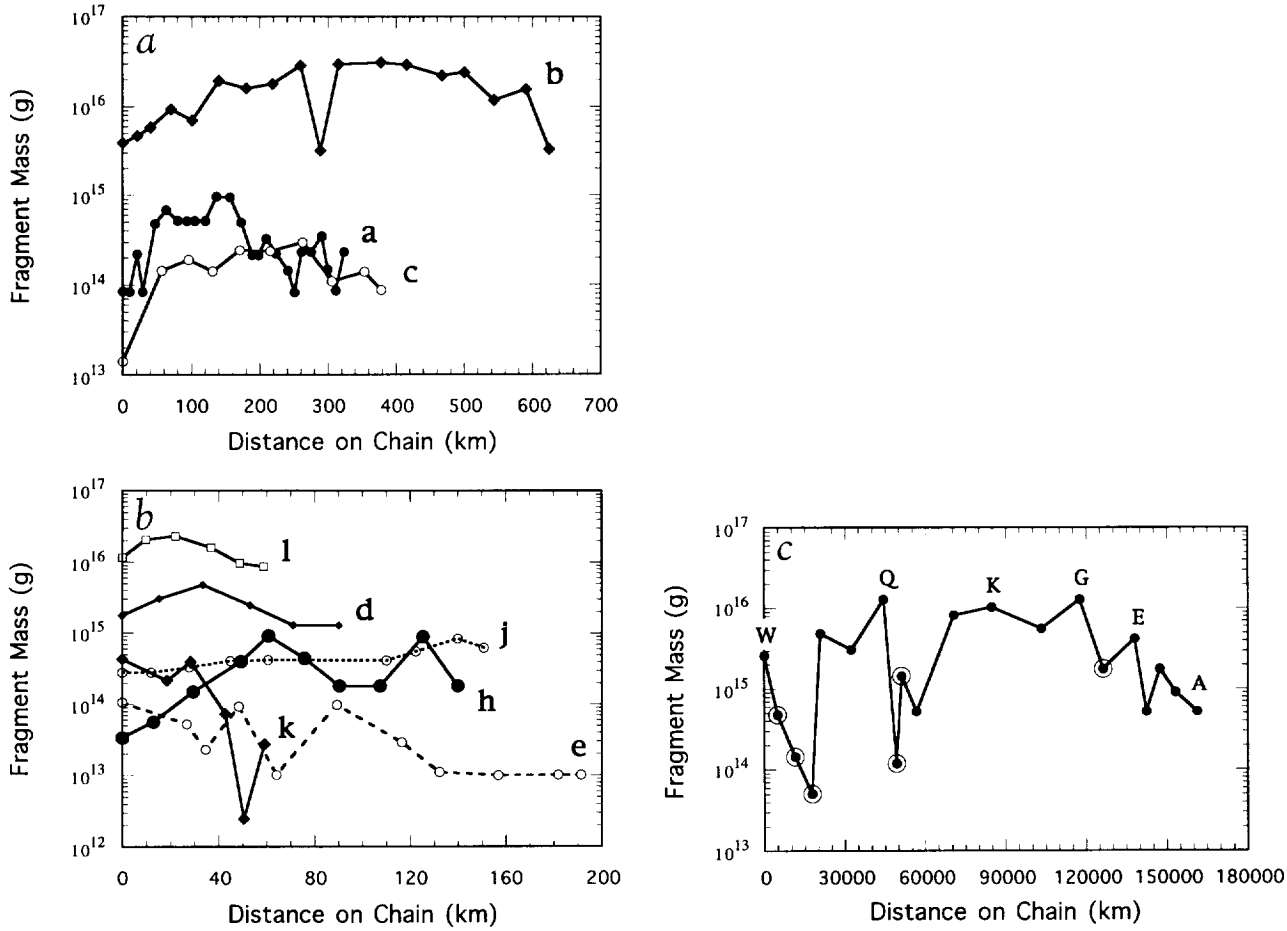

FIG. 8 (a, b). Derived fragment masses for individual comet fragments responsible for catena craters (McKinnon and Schenk 1995) as a function of crater location along each crater chain on Callisto and Ganymede. Each curve represents a separate crater chain, identified by letter (see Table I). Data are shown in two figures, with different scales, for clarity. Chains e, f, g, and j were poorly viewed by Voyager in comparison to the others. In the other chains, the largest fragments are located in the central section of each chain. (c) Relative fragment masses for prominent subnuclei (letters) of Shoemaker-Levy 9, shown in relation to their position along the fragment train as of July 1993 (Weaver *et al.* 1994). Masses estimated from derived relative nuclear diameters of Weaver *et al.* (1995), assuming $\rho = 0.6$ g/cm^3, and scaled for a parent body diameter of 2 km (Melosh and Schenk 1993). Circled fragments produced no observable effects on Jupiter. Compare with (a).

S–L9 parent body) by multiplying by 1.15, and diameter estimates by a factor of 1.24.

For the six most prominent and best observed crater chains, the largest fragments are located in the central section of each crater chain (Fig. 8). Fragments on the ends of crater chains are somewhat smaller. For the more poorly resolved crater chains, the case is less obvious, due in part to minor uncertainties in relative crater dimensions. Shortly after discovery of S–L9, it was apparent that the fragments nearer the center of the fragment train were brighter and probably larger than those at the ends (e.g., Weaver *et al.* 1994), with fragments G, H, K, L, and Q having the brightest apparent magnitudes. This conclusion was supported (with a few exceptions) by the magnitude of the observed corresponding impact scars on Jupiter (Weaver *et al.* 1995, Hammel *et al.* 1995). Weaver *et al.* (1995), using 1994 HST images, estimated relative radii for each nucleus, based on assumptions regarding the relationship between nuclear size and coma brightness. Their results, converted to masses assuming densities of 0.6 g/cm^3, are shown in Fig. 8c, with relative nuclear positions taken from the earlier July 1993 HST observations (Weaver *et al.* 1994), which give the highest resolution data at the earliest possible date. The largest fragments are located in the central section of the S–L9 train, similar to the pattern observed in crater chains (Figs. 8a, 8b).

Jupiter-Family Comets: Masses and Diameters

During the present epoch at least, short-period comets may dominate the impactor flux in the jovian system, with a contribution of up to 10% from long-period comets

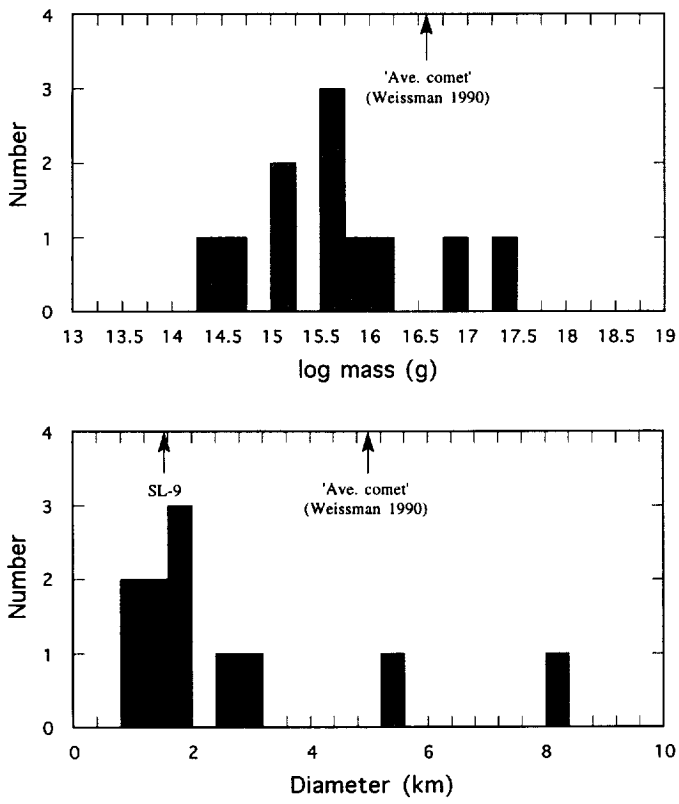

FIG. 9. Histograms of parent comet masses and diameters, for disrupted comets that have struck Callisto and Ganymede (McKinnon and Schenk 1995). Equivalent diameter derived assuming density of 1 g/cm^3. For comparison, the estimates of S–L9 parent comet diameter based on physical models of the breakup (Scotti and Melosh 1993, Asphaug and Benz 1994) and the average comet diameter estimate of Weissman (1990) are shown. Mean Halley diameter is ~11 km (Keller 1990).

(Shoemaker and Wolfe 1986, Shoemaker 1994). We infer that catenae represent a small sampling of the short-period (Jupiter-family) comet population (with perhaps a few long-period comets as well). Summing the fragment masses reported above for each catena (McKinnon and Schenk 1995) gives the total mass of each parent comet (Table II; Fig. 9). Parent comet masses range over three orders of magnitude, with a median mass of 3.8×10^{15} g. This is similar to the nominal comet mass employed by Asphaug and Benz (1994) in their disruption calculations. The largest fragment in each chain has a mass 0.1 to 0.38 that of the total comet mass, with an average value of $\sim 0.23 \pm 0.08$ (Fig. 10). There is no correlation between the mass of the parent comet and the number of fragments produced (Fig. 11) or with the length of the resulting crater chain (Tables I, II). However, there is a strong correlation between the mean fragment mass within a chain and the mass of the respective parent comet (Fig. 12).

While this crater chain comet sample is small, it does provide a consistency check on other comet mass and size estimates. McKinnon and Schenk (1995) estimated equivalent spherical diameters for catena parent comets associated with the anomalous crater chains (Table II), based on the estimated mass of each parent comet (above) and assumed densities of 1.0 g/cm^3. They also calculated equivalent parent comet diameters of 0.8 to 8.4 km, with a mean of 2.7 km (Fig. 9, Table II). Weissman (1990) estimates that long-period comets have a mean diameter of ~5 km (and mass of 3.8×10^{16} g, assuming densities of 0.6 g/cm^3). This is based on the observed population of long-period comets brighter than $H_{10} = 11$ ($D \geq 2$ km), and hence is observationally biased. Short-period comets may be somewhat smaller on average than long-period comets due to mass wastage during their many orbits around the Sun. Only six cometary nuclei have been observed "directly" (see review by Rahe *et al.* (1994)). These diameters range from ≤6 to 20 km (and up to ~300 km for Chiron). This sample is also observationally biased toward larger, less

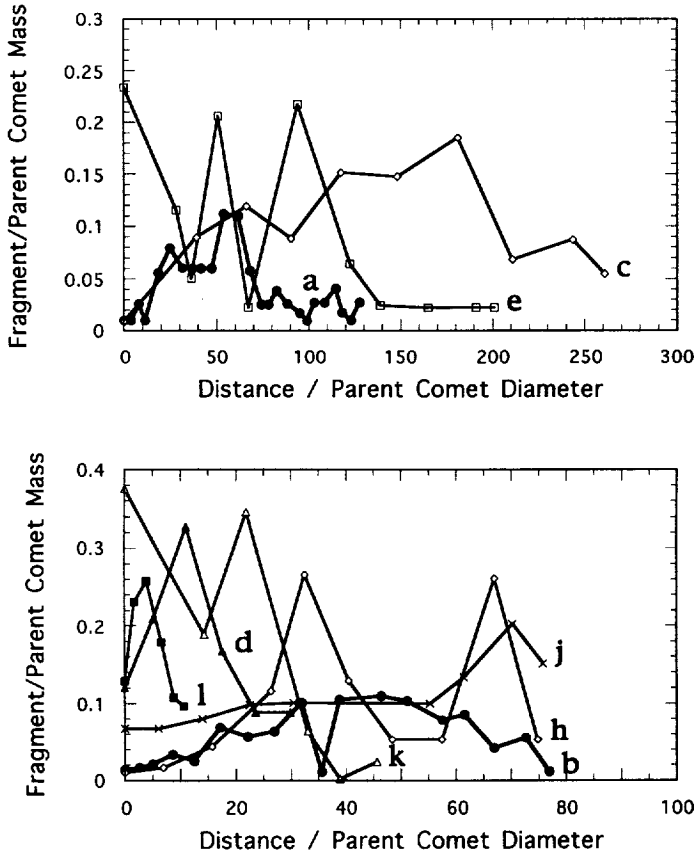

FIG. 10. Fragment mass, scaled to the total mass of the parent body, as a function of distance along the crater chain, scaled to the total length of the chain. Fragments masses are from McKinnon and Schenk (1995). The largest fragment in a chain has a mass ≤0.26 the mass of the parent comet, except for chains d and k, where the largest fragments are up to ~0.4 parent comet mass. Data are shown in two figures, with different scales, for clarity.

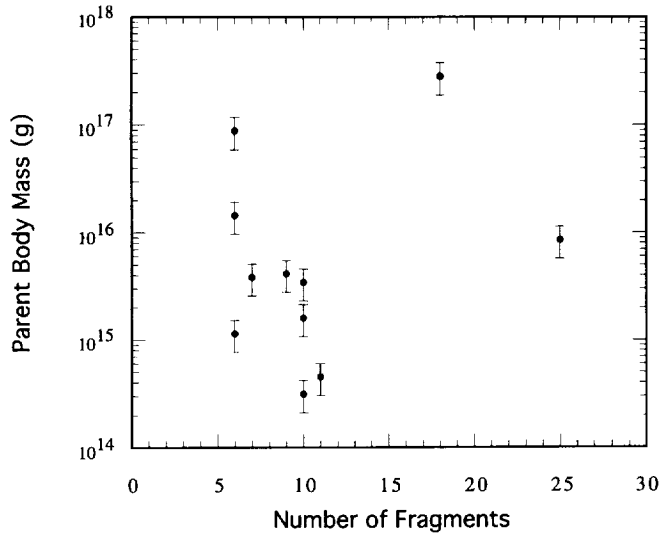

FIG. 11. Derived masses of parent comets (McKinnon and Schenk 1995) for crater chains on Callisto and Ganymede as a function of the number of fragments in each chain. No correlation is obvious.

active nuclei. The mean diameter of Comet Halley, measured from spacecraft imaging, is ~11 km (Keller 1990), larger than any of the crater chain parent comets.

Hubble Space Telescope (HST) observations of the S–L9 fragment train give upper limits of 2 to 4 km for the largest fragments, and an upper limit on the diameter of the S–L9 parent comet of ~8 km (Weaver *et al.* 1995). Hydrodynamic impact models of the entry of S–L9 fragments into Jupiter's atmosphere tend to favor small fragment sizes on the order of ≤800 m (e.g, Zahnle and MacLow 1995), consistent with a smaller parent body, although fragment diameters of up to ~2 km may be possible. Further modeling and data reduction may revise these estimates. Physical models of breakup also favor smaller fragment and parent comet diameters. Scotti and Melosh (1993), using a simple tidal splitting model, estimated a diameter for the parent comet of S–L9 of ~2 km (based on an early peri-Jove estimate of 1.6 R_J; using the corrected distance of 1.3 R_J gives a comet diameter of ~1.5 km using this method). Estimates based on rubble-pile fragmentation codes indicate an even smaller parent comet diameter of ~1 to 1.6 km (Solem 1994, Asphaug and Benz 1994). These values are similar to the diameters of crater chain parent comets (Fig. 9, Table II). If the S–L9 parent comet were much larger than 2 km across, it would be historically unusual in relation to the crater chain comet population. The catenae on the icy satellites represent only a very small sampling, however, of what must be a much larger population of comets historically disrupted by Jupiter. It is also plausible that this sample is biased toward relatively weak comets. If comets with sufficient strength to resist tidal disruption exist, they would not make crater chains.

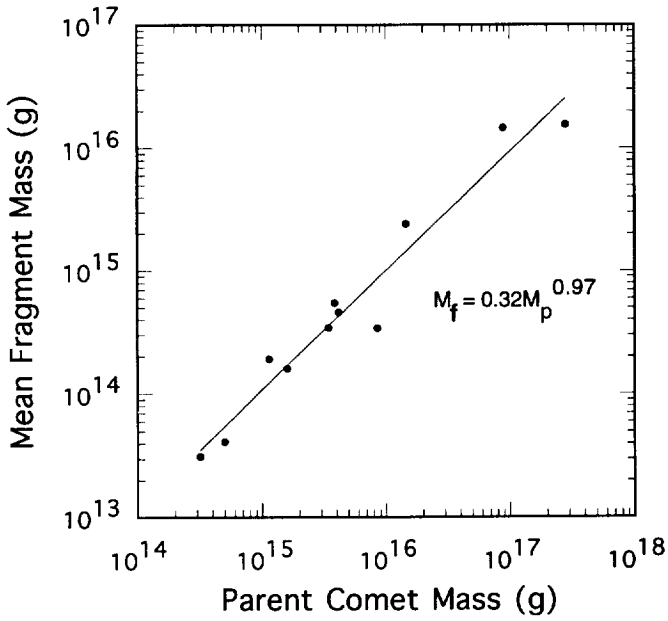

FIG. 12. Correlation of mean fragment mass for individual crater chain comets and mass of the associated parent comet (data from McKinnon and Schenk 1995).

DISCUSSION

Successful models for the structure and fragmentation of cometary nuclei should also account for the morphology of crater chains on the jovian satellites formed by disrupted comets. Three basic models have been developed for cometary nuclei: the "solid" or homogeneous nucleus (e.g., Sekanina 1996), the "cometesimal" nucleus consisting of roughly equal-sized fragments loosely bound by self-gravity (e.g., Scotti and Melosh 1993, Melosh and Schenk 1993), and the rubble pile nucleus consisting of many small fragments, possibly of varying sizes, also weakly bound by self-gravity (e.g., Weissman 1986, Asphaug and Benz 1994).

It has been demonstrated that tidal forces are insufficient to disrupt a solid nucleus with nonnegligible strength into multiple fragments (see Asphaug and Benz 1994, 1996). Melosh and Schenk (1993) proposed one explanation for the apparent similarity in crater sizes in the crater chains. They suggested that crater chain comets may have consisted of loosely bound roughly equidimensional cometesimals, which are separated during tidal breakup. Estimates of crater chain fragment masses (McKinnon and Schenk 1995) indicate that these putative cometesimals have an average diameter of 1.2 km, but vary in size by a factor of 10 or more (Table II). This variability in fragment dimensions is considerably more than suggested by crater dimensions alone (Melosh and Schenk 1993), because crater size

depends on other factors including impact velocity and geometry. Also, if the cometesimal nucleus model were applicable, fragment number should correlate directly with parent comet size, as more cometesimals would be required to construct a larger comet. There is no correlation of comet mass and the number of fragments produced by disruption in the crater chain record (Fig. 11). Essentially, the average fragment mass for a given chain should be roughly similar for all the crater chains independent of parent comet mass, contrary to what is observed (Fig. 12).

Comet Fragmentation: Can Rubble Pile Comets Make Crater Chains?

The S–L9 events led to the development of disruption models (Asphaug and Benz 1994, Solem 1994, Olson and Mumma 1994) based on the rubble pile or fractal concept of cometary nuclei (e.g., Donn *et al.* 1985, Weissman 1986). The rubble pile model proposes that comet nuclei are composed of many individual particles which have internal strength but little or no cohesive strength with respect to their neighbors. Passage through the Roche zone disrupts this assemblage into a highly elongated body, which becomes gravitationally unstable and reassembles into a line of clusters (or aggregates of particles) smaller than the parent body (e.g., Asphaug and Benz 1994, Solem 1994).

Rubble pile models make testable predictions regarding the relative spacing, dimensions, and shapes of cometary chains and their fragments (e.g., Solem 1994, Asphaug and Benz 1996). Numerical simulations of the disruption of rubble pile comets that produce S–L9 morphologies produce clusters with relatively uniform mass, but this "typical" mass varies as a function of comet density and encounter distance to the planet (e.g., Asphaug and Benz 1996). We observe that the mean fragment mass varies considerably from chain to chain but with no apparent correlation to any measurable variable, such as parent comet mass. Encounter distances (and densities) are unknown for the comets that produced these crater chains and could easily account for the observed variations in mean fragment mass from chain to chain. The largest clusters in each simulation contain on average ~0.2 the total mass of the parent comet, very similar to the average value of ~0.23 for the crater chains (Fig. 10). The larger clusters are found in the central section of disrupted comet chains, and the nature of the gravitational instabilities in these disruption models tends to produce clusters that are more or less evenly spaced (e.g., Asphaug and Benz 1994). These also are patterns similar to those seen in the crater chains and S-L9 (Fig. 8). Overall, these correlations suggest that the distribution of material within a given crater chain is similar to that predicted by rubble pile calculations. The lack of correlation between parent body mass and number of fragments is also consistent with rubble pile simulations (e.g., Asphaug and Benz 1996), because the number of fragments or clusters formed is a function of encounter distance from Jupiter (assuming constant density). We conclude that the morphology of crater chains on Callisto and Ganymede is most consistent with the morphology predicted for disruption of cometary nuclei constructed as rubble piles (e.g., Asphaug and Benz 1994, 1996).

The strong correlation between mean fragment mass and parent comet mass (Fig. 12) suggests that breakups are self-similar and scale invariant (e.g., Solem 1994, Asphaug and Benz 1996). Unless large comets are formed from proportionally larger cometesimals, the cometesimal model for comet nuclei is incapable of explaining such a correlation. Rubble piles, on the other hand, break up naturally in a self-similar fashion. Asphaug and Benz (1996) show that for a fixed peri-Jove, the number of clumps that form depends only on comet density, and not diameter. All other factors being equal, larger rubble piles break up into the same number of clumps, except that the clumps are larger and form longer chains. This implies that the effective grain sizes of comets are much smaller than the clusters which form after disruption (Asphaug and Benz 1994).

The remarkable alignment of craters within crater chains indicates that the clusters forming the craters are essentially coplanar at impact. A characteristic of the rubble-pile simulations is that there are no forces (except possibly collisional) acting to form or pull clusters out of the comet's orbital plane. The alignment of craters within crater chains suggests that it would be necessary to damp out any components of cluster velocity perpendicular to the orbit plane of the comet. Whatever forces pushed S–L9 fragments (such as B and F) "offline" late in S–L9 evolution (e.g., Weaver *et al.* 1994) evidently do not have time to force clusters offline by the time they strike Ganymede or Callisto; otherwise, zigzag crater patterns would be evident on these satellites. A full treatment of this issue is beyond the scope of this work, however.

The S–L9 string-of-pearls morphology is not the only comet train morphology predicted by rubble pile models. The number of clusters and the morphology of comet chains produced by tidal disruption is a function of comet density and the ratio of the peri-Jove distance to the Roche limit radius, which is a function of planetary density (e.g., Asphaug and Benz 1996). For a passing comet with a large peri-Jove (or with a relatively high density), most of the mass will reaccrete into one or two central condensations with only a fraction of the mass located in tails extending to either side. A large crater formed by this central condensation and its extensive ejecta will tend to obliterate the effects of any low-mass tails. As a result, the possible impact of this type of disrupted comet is not well constrained by the satellite cratering record. For comets passing close to Jupiter (or those with unusually low densities), the rub-

ble pile will rip apart into an extremely long pencil-shaped structure, which will not have time to reaccrete into distinct clusters by the time it passes Callisto. For a nominal density of 0.6 g/cm^3, the peri-Jove distance required to produce this morphology is below the cloud decks (Asphaug and Benz 1996) and is consistent with the lack of evidence for the impact of such pencil-shaped objects on either satellite. To date, only the S–L9-type morphology has been recognized on Ganymede or Callisto. The number of clusters formed in intermediate cases (i.e., the string-of-pearls morphology) varies with peri-Jove distance (or density or nucleus rotation), and this may be reflected in the variations in fragment numbers seen in crater chains (Table I).

Rubble Pile Clusters and Crater Morphology

The disruption of rubble-pile comets can produce strings of reassembled condensations or clusters. If particle collisions are dissipative, these clusters can be tightly packed and have densities approaching that of the parent comet (e.g., Richardson *et al.* 1995). In the "swarm" variant of the rubble pile model, particles are dispersed in large diffuse clusters, or swarms, with low effective bulk density (e.g., Rettig *et al.* 1994). Loosely clustered projectiles produce craters that are anomalously shallow and have irregular rim outlines and pitted and ridged floor morphologies compared to solid projectile crater morphology (O'Keefe and Ahrens 1982, Schultz and Gault 1985). This results from the interference of simultaneous, adjacent shock waves.

If we assume that clustered impact experiments (e.g., Schultz and Gault 1985) can be extrapolated generally to planetary scales, we may be able to place loose constraints on the dispersion of the impacting rubble pile clusters based on observed crater morphology. The impact experiments (in the strength regime) suggest that crater depth/diameter ratios begin to flatten out when the ratio of projectile-to-target density is less than ~0.1 (Fig. 15 in Schultz and Gault 1985). We take Gomul Catena as a representative example, which has an average crater diameter of 14 km and an estimated mean fragment mass of 3.4×10^{14} g (ρ = 1 g/cm^3) and mean fragment diameter of 0.8 km (Table II). (We assume a target density of 1 g/cm^3.) If the particles are dispersed uniformly into a spherical cloud such that the effective density of an average fragment (or cluster) is only 0.1 g/cm^3, this cluster would have an effective diameter of ~2 km, or roughly 0.14 times the observed mean crater diameter (D) for this chain. Catena crater depths and morphology are generally consistent with those of ordinary craters. Dispersed clusters much larger than approximately 0.14D (or ~2 km for Gomul Catena) would be expected to produce unusual crater morphologies (e.g., Schultz and Gault 1985).

The tidal disruption model of Asphaug and Benz (1994) produces clusters that can have dispersed halos of particles. These halos can be up to ~4 km in diameter, somewhat larger than the estimated maximum allowable cluster size of ≤2 km (for Gomul Catena). Most of the mass in their clusters is concentrated in a central condensation only 1–1.5 km across, which is allowed by crater chain morphology. The Asphaug and Benz tidal model lacks dissipation, potentially overestimating the diffusiveness of the reaccreted clusters. By making collisions more dissipative in the models, clusters can condense much faster (at <8 R_J) and more tightly, such that cluster density resembles that of the parent comet (Olson and Mumma 1994, Richardson *et al.* 1995). Even with a halo of particles (provided it has much less mass than the central condensation), we expect rubble pile clusters to produce craters with generally normal appearances (at Voyager resolution) of the type observed. (Some irregular morphologies may result due to interference by closely spaced craters, independent of fragment morphology.)

High-resolution Galileo images of small-scale (<0.2 km) morphologic details may reveal or exclude indications of clustered impacts (e.g., irregular floor morphology, small subsidiary cratering events). Observations of this type may provide a more robust constraint on how tightly fragment clusters are constructed. High-resolution imaging of catena craters and ejecta is also desirable for determining sequence of impact within each chain in order to assess likely comet trajectories (cf. McKinnon and Schenk 1995). Improved resolution on crater chains poorly seen by Voyager (especially Gunntro and Enki Catenae) is also required to better characterize crater sizes. High resolution comparison of chains on Callisto and Ganymede could provide indications of how comet fragment trains evolve as they move away from Jupiter. The gaps in the Voyager's global imaging surveys of these satellites should be filled at ≤1 km/pixel resolution to complete the global inventory of anomalous crater chains. Unfortunately, the communications-challenged Galileo orbiter will be able to address only some of these issues. As of this writing, high-resolution observations of crater chains are scheduled only for a portion of Gomul Catena. Improved resolution is also anticipated for Eikin, Gunntro, and possibly Svol Catenae, all on Callisto.

Comparison with Shoemaker–Levy 9: What if S–L9 Had Struck Callisto?

Shoemaker–Levy 9 represents the only observed disrupted comet that can be compared with crater chains directly (P/Brooks 2 was discovered too long after disruption for useful comparison). Changes in coma brightness and nuclear position with time indicate that a few S–L9 nuclei were less substantial than initially thought, continued to break up over time, or disappeared altogether (e.g., Weaver *et al.* 1994). Some observed nuclei (e.g., F, P1, T,

and U) produced negligible effects during the collision with Jupiter (Hammel *et al.* 1995) and it is not clear what the physical state of these objects was in the days immediately after disruption in 1992. Crater chains on Ganymede and Callisto formed within hours after fragmentation (Melosh and Schenk 1993). S–L9, however, was discovered eight months after it had passed Callisto's orbit and long-term evolution of the nuclei may complicate comparison with the crater chains.

For a comparison of S–L9 with catenae on the jovian satellites, we have attempted to reconstruct the crater chain that this comet would have produced if it had struck Callisto in July 1992. We use the relative fragment dimensions of Weaver *et al.* (1995) to estimate fragment masses, scaling these values so that a parent comet with density 0.6 g/cm^3 and diameter 2 km (Scotti and Melosh 1993, Asphaug and Benz 1994) results. For a 2-km-wide comet passing at 1.3 R_J, the resulting crater chain on Callisto is expected to be on the order of 350 km long (Melosh and Schenk 1993). Orbital integrations of S–L9 are not currently accurate enough to be used to predict relative fragment positions when S–L9 first crossed Callisto's orbit. The relative fragment positions used above (Fig. 8c) were scaled to give relative crater positions in our 350-km crater chain on Callisto. To estimate crater sizes for each fragment, we reverse the scaling calculation used to estimate fragments masses for catena craters (McKinnon and Schenk 1995). Hypothetical impact angles for the S–L9 fragments are unconstrained, as we do not know where on Callisto they might have hit; we assume 45°. Otherwise, we assume parameters similar to those used by McKinnon and Schenk.

Figure 13a shows the putative crater chain that might have been expected from S–L9, with uncertainties of a factor of two or less in the sizes and positions of each crater. Interestingly, some of the smaller craters are "swallowed" up by larger neighbors. The smaller craters produced by fragments P2 and Q2 are obliterated by P1 and Q1. The fragments that produced insignificant effects on Jupiter (F, G2, P1, P2, T, U, V; Hammel *et al.* 1995) may also have produced small or negligible craters on Callisto. If we eliminate these fragments, we find a reasonable match of this model crater chain (Fig. 13b) to observed crater chain characteristics, especially Gomul and Gipul Catenae (Tables I, II; Figs. 1a, 1b). For example, the diameter of the smallest crater is within a factor of 2.5 of the largest crater. Spacing is relatively uniform and varies within a factor 3 (Table I). The largest craters are in the central section of the chain as expected (see also Fig. 8c). The large fragments in the central region produce craters that are separated or overlap by less than 5 km, as seen in crater chains. A few craters have considerable overlap, particularly the crater for fragment D, but some of the associated S–L9 fragments (B, D, N, and Q2) produced only minor atmospheric effects on Jupiter (Hammel *et al.* 1995) and the sizes of these craters may be overestimated. Closely spaced fragments could produce larger "merged" craters similar to that seen at Nanshe Catena (Fig. 1l), or the somewhat elongate craters seen at Gipul Catena (Fig. 1b). Despite some uncertainties, the relative spacing and masses of fragments within the S–L9 fragment train is remarkably similar to that within crater chains on the jovian satellites (Fig. 8; Tables I, II), and that predicted by rubble pile disruption models (e.g., Solem 1994, Asphaug and Benz 1994). It is apparent that S–L9 would have made a fine crater chain on Callisto (Fig. 13b).

The process in which larger craters can obliterate small adjacent craters (Fig. 13a) may occur in crater chains. If so, it could be a factor in the large intercrater spacing in chains such as Gipul Catena, and the paucity of craters <5 km across in chains (if they ever formed). The possibility that a few small fragments were obliterated by craters from larger fragments should be considered when evaluating crater chain morphology. The masses of these small fragments are probably negligible, however; otherwise, a greater number of oblong or elliptical craters would be apparent.

At the time of discovery, optically prominent "dusty" wings extended thousands of kilometers beyond the observed nuclei. By July 1994, these wings had largely dispersed or faded (Weaver *et al.* 1995). Such dust wings, particularly in the early phase of disrupted comet evolution, may have sufficient mass to disturb the regolith of an icy satellite during impact. No evidence for the impact of such wings is apparent in the Voyager images (e.g., Figs. 1j, 1l). These dust wings would have been much shorter in July 1992 than when observed in 1993. The effects on satellite surfaces may be subtle, however, requiring photometric or color mapping to be detectable. Crater ejecta would obliterate a significant portion of any such deposit, however.

CONCLUSIONS

Anomalous crater chains on Callisto and Ganymede represent a record of tidally disrupted comets and reveal a number of important characteristics about comet nuclei and disruption processes. An average of 11 craters formed per disruption event, but can range from 6 to 25. Spacing between craters in each chain is uniform within a factor of 2. Estimated fragment masses (Table II) are relatively uniform for each disruption event but vary by at least 4 orders of magnitude between the disruption events sampled by crater chains (McKinnon and Schenk 1995). The largest fragments are generally located in the center portion of chains, and the largest fragment in a given chain is ~0.23 times the mass of the parent comet (Fig. 10). There is no correlation observed between the number of fragments per disruption event and parent comet mass, but

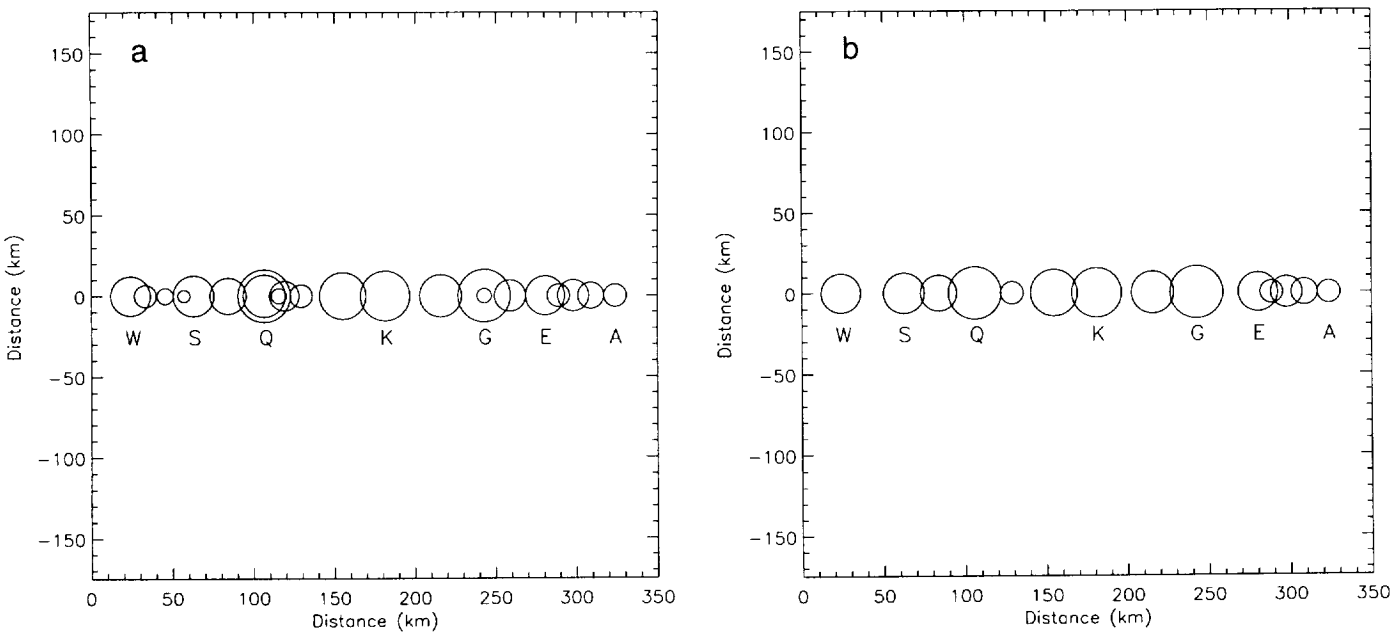

FIG. 13. (a) Model of crater chain that might have been produced by S–L9, had it struck Callisto in July 1992. Model crater sizes are based on the relative fragment sizes estimated from HST images (Weaver *et al.* 1995), assuming density of 0.6 g/cm^3, and scaled for a comet with a diameter of 2 km. Relative positions are scaled to a chain of 350 km length at Callisto (from Fig. 8c, Weaver *et al.* 1994). We also assume a linear comet chain. (b) Version of (a) shown after removal of fragments F, P1, P2, T, U, and V, which produced no observed effect on Jupiter's atmosphere (Hammel *et al.* 1995). We note that fragments B, D, N, and Q2 also produced relatively minor effects, and their masses (and crater sizes) may have been overestimated.

there is a strong correlation between parent comet mass and mean fragments mass (Fig. 12). Crater morphology also indicates that individual fragment clusters are relatively tightly packed (roughly $\leq 0.14D$) by the time they strike the outer galilean satellites, although the degree of compaction required is weakly constrained at present.

The observed properties of ancient disrupted comets as recorded on the galilean satellites are most consistent with predictions of rubble pile disruption models (e.g., Asphaug and Benz 1994), and with the observed properties of S–L9 (Weaver *et al.* 1995). It is clear that each disruption event is different in terms of the number of fragments produced and their mass, but this variation is also consistent with the predictions of rubble pile calculations, and is related to the encounter distance, density and rotation of the comet (e.g., Asphaug and Benz 1996). These crater chains represent a small sampling of disrupted short-period (and perhaps a few long-period) comets, although if "strong" comets exist and fail to disrupt after passing close to Jupiter, they would not be represented in this sample. The estimated frequency with which these comets are disrupted by Jupiter, 1 every 275 ± 100 years, is consistent with other estimates (e.g., Shoemaker 1995). Although limited, Galileo observations of crater chains on the jovian satellites will be critical to extending our understanding of disrupted comet populations and characteristics.

ACKNOWLEDGMENTS

The authors thank Julie Moses, Stan Peale, Peter Schultz, Clark Chapman, and an anonymous reviewer for their comments and reviews. A portion of this work was performed at the Jet Propulsion Laboratory under contract with NASA. Lunar and Planetary Institute Contribution 886.

REFERENCES

ALLEN, C. C. 1979. Large lunar secondary craters: Size-range relationships. *Geophys. Res. Lett.* **6,** 51–54.

ASPHAUG, E., AND W. BENZ 1994. Density of comet Shoemaker–Levy 9 deduced by modelling breakup of the parent "rubble pile." *Nature* **370,** 120–124.

ASPHAUG, E., AND W. BENZ 1996. Size, density and structure of Comet Shoemaker–Levy 9 inferred from the physics of tidal breakup. *Icarus,* **121,** 225–248.

BENNER, L. A. M., AND W. B. MCKINNON 1995. On the orbital evolution and origin of Comet Shoemaker–Levy 9. *Icarus* **118,** 155–168.

CROFT, S. K., J. S. KARGEL, R. L. KIRK, J. M. MOORE, P. M. SCHENK, AND R. G. STROM 1995. The geology of Triton. In *Neptune and Triton* (D. P. Cruikshank, Ed.), pp. 879–947. Univ. of Ariz. Press, Tucson.

DONN, B., P. A. DANIELS, AND D. W. HUGHES 1985. On the structure of the cometary nucleus. *Bull. Am. Astron. Soc.* **17,** 520.

GAULT, D. E., J. E. GUEST, J. B. MURRAY, D. DZURISIN, AND M. C. MALIN 1975. Some comparisons of impact craters on Mercury and the Moon. *J. Geophys. Res.* **80,** 2444–2460.

HALFEN, C. W., P. H. SCHULTZ, AND D. E. GAULT 1990. Origin of anoma-

lous crater chains and their implications for the cratering record. *Proc. Lunar Planet. Sci. Conf. 21st,* 447–448.

HAMMEL, H. B., AND 16 COLLEAGUES 1995. HST imaging of atmospheric phenomenon created by the impact of Comet Shoemaker–Levy 9. *Science* **267,** 1288–1296.

JENSEN, J. R. 1986. *Introductory Digital Image Processing.* Prentice–Hall, New York.

KARGEL, J. S., AND S. POZIO 1996. The volcanic and tectonic history of Enceladus. *Icarus* **119,** 385–404.

KELLER, H. U. 1990. Surface features and activity of Comet Halley. In *Comet Halley: Investigations, Results, and Interpretations* (J. Mason, Ed.), pp. 133–145. Horwood, New York.

LUCCHITTA, B., AND L. SODERBLOM 1982. The geology of Europa. In *Satellites of Jupiter* (D. Morrison, Ed.), p. 521–555. Univ. of Ariz. Press, Tucson.

MARSDEN, B. 1989. The sungrazing comet group. II. *Astron. J.* **98,** 2306–2321.

MCKINNON, W. B., AND E. M. PARMENTIER 1986. Ganymede and Callisto. In *Satellites* (J. A. Burns and M. S. Matthews, Eds.), pp. 718–763. Univ. of Ariz. Press, Tucson.

MCKINNON, W. B., AND P. M. SCHENK 1995. Estimates of comet fragment masses from crater chains on Callisto and Ganymede. *Geophys. Res. Lett.* **13,** 1829–1832.

MELOSH, H., AND P. SCHENK 1993. Split comets and the origin of crater chains on Ganymede. *Nature* **365,** 731–733.

MELOSH, H. J., AND E. A. WHITAKER 1994. Split comets and crater chains on the Moon. *Nature* **369,** 713–714.

MOORE, J. M. 1984. The tectonic and volcanic history of Dione. *Icarus* **59,** 205–220.

MOORE, J. M., V. M. HORNER, AND R. GREELEY 1985. The geomorphology of Rhea. *J. Geophys. Res.* **90,** C785–C795.

OBERBECK, V. R., AND R. M. MORRISON 1974. Laboratory simulation of the herringbone pattern associated with lunar secondary crater chains. *Moon* **9,** 415–455.

O'KEEFE, J. D., AND T. J. AHRENS 1982. Cometary and meteorite swarm impact on planetary surfaces. *J. Geophys. Res.* **87,** 6668–6680.

OLSON, K. M., AND M. J. MUMMA 1994. Simulations of the breakup and dynamical evolution of Comet Shoemaker–Levy 9 employing a swarm model. *Bull. Am. Astron. Soc.* **26,** 1574–1575.

PASSEY, Q. R., AND E. M. SHOEMAKER 1982. Craters and basins on Ganymede and Callisto: Morphological indicators of crustal evolution. In *Satellites of Jupiter* (D. Morrison Ed.), pp. 379–434. Univ. of Ariz. Press, Tucson.

RAHE, J., V. VANYSEK, AND P. R. WEISSMAN 1994. Properties of cometary nuclei. In *Hazards Due to Comets and Asteroids* (T. Gehrels, Ed.), pp. 597–634. Univ. of Ariz. Press, Tucson.

RETTIG, T. W., J. M. HAHN, S. C. TEGLER, M. J. MUMMA, AND M. DISANTI 1994. Hubble Space Telescope observations of Comet Shoemaker–Levy 9 subnuclei: Solid bodies or swarms. *Bull. Am. Astron. Soc.* **26,** 1567.

RICHARDSON, D. C., E. ASPHAUG, AND L. BENNER 1995. Comet Shoemaker–Levy 9: A "rubble pile" model with dissipative collisions and gravitational perturbations. *Bull. Am. Astron. Soc.* **27,** 1114.

SCHENK, P. M. 1991. Ganymede and Callisto: Complex crater formation and planetary crusts. *J. Geophys. Res.* **96,** 15,635–15,664.

SCHENK, P. M. 1993. Central pit and dome craters: Exposing the interiors of Ganymede and Callisto. *J. Geophys. Res.* **98,** 7475–7498.

SCHENK, P. M. 1995. Geology of Callisto *J. Geophys. Res.* **100,** 19,023–19,041.

SCHENK, P. M., AND W. B. MCKINNON 1987. Ring geometry on Ganymede and Callisto. *Icarus* **72,** 209–234.

SCHULTZ, P. H. 1976. *Moon Morphology.* Univ. of Texas Press, Austin.

SCHULTZ, P. H., AND D. E. GAULT 1985. Clustered impacts: Experiments and implications. *J. Geophys. Res.* **90,** 3701–3732.

SCOTTI, J. V., AND H. J. MELOSH 1993. Estimate of the size of Comet Shoemaker–Levy 9 from a tidal breakup model. *Nature* **365,** 733–735.

SEKANINA, Z. 1982. The problem of split comets in review. In *Comets* (L. L. Wilkening, Ed.), pp. 251–287. Univ. of Ariz. Press, Tucson.

SEKANINA, Z. 1996. Tidal breakup of Comet Shoemaker–Levy 9. In *Proc. of IAU Colloquium 156.* Columbia Univ. Press, in press.

SEKANINA, Z., AND D. K. YEOMANS 1985. Orbital motion, nucleus precession, and splitting of periodic comet Brooks 2. *Astron. J.* **90,** 2335–2352.

SHOEMAKER, E. M. 1994. Update on the impact rates in the jovian system. Paper presented at *Icy Galilean Satellites: An International Conference.* San Juan Capistrano Institute, San Juan Capistrano, CA.

SHOEMAKER, E. M. 1995. Comet Shoemaker–Levy 9 at Jupiter. *Geophys. Res. Lett.* **22,** 1555–1556.

SHOEMAKER, E. M., AND R. F. WOLFE 1982. Cratering time scales for the Galilean satellites. In *Satellites of Jupiter* (D. Morrison, Ed.), pp. 277–339. Univ. of Ariz. Press, Tucson.

SOLEM, J. C. 1994. Density and size of Comet Shoemaker–Levy 9 deduced from a tidal breakup model. *Nature* **370,** 349–351.

SPENCER, J., AND P. R. MALONEY 1984. Mobility of water ice on Callisto: Evidence and implications. *Geophys. Res. Lett.* **11,** 1223–1226.

THOMAS, P. 1979. Surface features of Phobos and Deimos. *Icarus* **40,** 223–243.

WEAVER, H. A., AND 18 COLLEAGUES 1994. Hubble Space Telescope observations of Comet P/Shoemaker–Levy 9 (1993e). *Science* **263,** 787–791.

WEAVER, H. A., AND 20 COLLEAGUES 1995. The Hubble Space Telescope observing campaign on Comet P/Shoemaker–Levy 9. *Science* **267,** 1282–1288.

WEISSMAN, P. R. 1986. Are cometary nuclei primordial rubble piles? *Nature* **320,** 242–244.

WEISSMAN, P. R. 1990. Cometary impactor flux at the Earth. In *Global Catastrophes in Earth History,* Geol. Soc. Am. Spec. Paper 247, pp. 171–180.

WICHMAN, R. W., AND C. A. WOOD 1995. The Davy crater chain: Implications for tidal disruption in the Earth–Moon system and elsewhere. *Geophys. Res. Lett.* **22,** 583–586.

WILHELMS, D. E. 1987. The geologic history of the Moon. U.S. Geol. Surv. Prof. Paper 1348.

WORONOW, A., R. STROM, AND M. GURNIS 1986. Interpreting the cratering record: Mercury to Ganymede and Callisto. In *Satellites* (J. A. Burns and M. S. Matthews, Eds.), pp. 237–276. Univ. of Ariz. Press, Tucson.

ZAHNLE, K., AND M.-M. MACLOW 1995. A simple model for the light curve generated by a Shoemaker–Levy 9 impact. *J Geophys. Res.* **100,** 16,885–16,894.